Reliability Engineering and System Safety 241 (2024) 109689

Contents lists available at ScienceDirect

Reliability Engineering and System Safety

journal homepage: www.elsevier.com/locate/ress

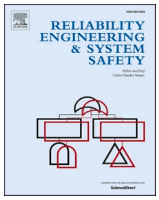

Modelling standoff distances to prevent escalation in shooting attacks to tanks storing hazardous materials

Matteo Iaiani, Riccardo Sorichetti, Alessandro Tugnoli, Valerio Cozzani *

LISES – Laboratory of Industrial Safety and Environmental Sustainability, DICAM, University of Bologna, via Terracini n. 28, 40131, Bologna, Italy

ARTICLE INFO

Keywords:
Security
Chemical and process industry
Shooting
Standoff distance
Projectile impact
Angle of impact
Ballistic limit velocity

ABSTRACT

Industrial equipment storing hazardous substances can be the target of deliberate malicious attacks causing escalation scenarios involving the release of flammable and/or toxic material with severe consequences on people, assets, and the environment. In the present study, a novel modelling approach was developed to assess the baseline values of standoff distances for atmospheric and pressurized storage equipment considering a set of standardized handgun and rifle projectiles not specific for military uses. The calculation of standoff distances is based on specific models for projectile perforation and flight. The range of standoff distances varies depending on the type of firearm used. Standoff distances resulted in the range of less than 10 m in case of handgun projectiles and up to 1130 m in case of hard-core rifle projectiles. Important differences in standoff distances were found for atmospheric and pressurized tanks. The effect of the initial offset angle of the shooter on the standoff distance was assessed by a Monte Carlo analysis based on credible offset angles for handgun and rifle projectiles. A case study demonstrates the importance of the results to improve chemical site security with respect to attack detection, emergency response, and mitigation actions aimed at preventing escalation scenarios.

1. Introduction

Atmospheric and pressurized equipment storing hazardous materials (e.g., flammable, toxic materials) may be the target of deliberate malicious attacks aimed at triggering escalation scenarios (release of hazardous material and/or energy) [1–3] with potential for severe consequences on workers, population, property, the environment, and company reputation [4–6].

The analysis of an extended dataset of past security-related events affecting the Chemical and Process Industry (CPI) performed by Casson Moreno et al. [7] and by Iaiani et al. [8,9] evidenced a significant increase in the number of reported events after year 2000 and confirmed the relevance and severity of security attacks in the CPI and in related industrial sectors (e.g., the Oil&Gas industry). This issue is also evidenced by other authors: e.g., Chen et al. [10] and Zhu et al. [11] point out that chemical and process plants, and in particular chemical industrial parks where large amounts of flammable materials (e.g., liquefied natural gas, crude oil, etc.) are stored, are susceptible to cascading events triggered by deliberate malicious attacks. In such events, the consequences of a primary event may escalate and cause the damage of nearby units, possibly triggering one or more secondary events leading to overall consequences more severe than those of the primary event [12]. Historical evidence shows the use of simple tools, as incendiary and explosive devices, as well as shooting with both light weapons (e.g., handguns and rifles) and heavy weapons (e.g., missiles) in deliberate attacks to chemical and process plants [8,13,14].

Though regulations addressing the security of installations storing and/or processing hazardous materials are quite different worldwide [15], the risks associated to deliberate malicious attacks (security attacks) are typically addressed using Security Vulnerability Assessment (SVA) or Security Risk Assessment (SRA) methodologies to determine the adequacy of existing security measures (security barriers) and the actual level of the security risk of a facility [16,17]. SVA/SRA methodologies suitable for the CPI and similar sectors span from qualitative or semi-quantitative approaches (e.g., the CCPS methodology [18], the VAM-CF methodology [19], the methodology proposed by API RP 780 [20], the RAMCAP methodology [21], the methodology developed by the Hazardous Incidents Commission [14], etc.) to quantitative approaches, based on static Bayesian Networks [22,23], on dynamic Bayesian Networks [4], on game theory [24–26], on dynamic graph theory [10,27], on fuzzy logic [28], and on event tree analysis [29].

Shooting attacks are considered a possible attack mode that can be perpetrated by the adversaries by all the aforementioned SVA/SRA

* Corresponding author.
E-mail address: valerio.cozzani@unibo.it (V. Cozzani).

https://doi.org/10.1016/j.ress.2023.109689
Received 25 February 2023; Received in revised form 4 August 2023; Accepted 23 September 2023
Available online 30 September 2023
0951-8320/© 2023 The Author(s). Published by Elsevier Ltd. This is an open access article under the CC BY license (http://creativecommons.org/licenses/by/4.0/).

Nomenclature

AP	Armour-Piercing
CPI	Chemical and Process Industry
DBT	Design Basis Threat
FN	Flat Nose
HC	Hard-Core
MOA	Minute Of Angle
P	Pointed
PE	Probability of Exceedance
PM	Perforation Model
PPS	Physical Protection System
RN	Round Nose
S	Spherical
SC	Soft-Core
SOD	StandOff Distance
SRA	Security Risk Assessment
SVA	Security Vulnerability Assessment
TE	Target Element
t	Target actual thickness
t_{max}	Target maximum perforated thickness
t_{eff}	Target effective thickness
t_d	Target thickness by design
θ	Impact angle (polar angle in a spherical coordinate system with the impact point as origin and the normal to the target wall as polar axis)
β	Azimuthal angle of the impact point on the vessel (azimuthal angle in a cylindrical coordinate system with the axis of the vessel as refence axis and the direction aimed by the shooter as reference direction for the azimuth)
ϕ	initial offset angle (polar angle in a spherical coordinate system with the shooter as origin and the direction aimed by the shooter as polar axis)
ϕ_r	reference initial offset angle
δ	Initial azimuthal angle (azimuthal angle in a spherical coordinate system with the shooter as origin, the direction aimed by the shooter as polar axis and the direction parallel to the vessel axis as reference direction for the azimuth)
m	Projectile mass
d	Projectile diameter
D	Vessel diameter
H	Maximum design liquid level
P_d	Vessel design pressure
V	Vessel volume
u_b	Ballistic limit velocity (minimum velocity of the projectile at the impact point that causes perforation)
$u_{b,n}$	Normal component of ballistic limit velocity
d_r	Downrange distance (distance from the shooter to the target)
u_m	Muzzle velocity (velocity of the projectile at the shooting point)
ρ	Density
BHN	Brinell's hardness number
σ_T	Target yield stress
σ_R	Target tensile stress
G	Target shear modulus
Y	Target flow stress or dynamic yield stress
E	Target Young modulus
f	Friction coefficient
τ_S	Target static shear strength
υ	Target Poisson ratio
α	Projectile half-angle of conical nose
K	Target bulk modulus
p	Subscript for projectile
t	Subscript for target

methodologies since they may damage industrial equipment and storage tanks even from long distances. The potential for shooting attacks of damaging chemical and process equipment was also confirmed by the past incident analysis performed in previous studies by Casson Moreno et al. [7] and by Iaiani et al. [8].

According to the "Rings of Protection" or "layered defence" principles [18,30], the concept of "standoff distance" is applicable in the security domain in order to investigate the conditions for a successful attack and to support the design of passive protection barriers within the Physical Protection System (PPS) of a facility. The standoff distance is the minimum distance between the target asset and the location of the adversary that will not cause any significant damage to the target [31]. Actually, most attack vectors decrease their intensity with distance (e.g., heat load for incendiary attacks, overpressure for attacks involving explosives, projectile velocity for shooting attacks, etc.), until they are no longer able to damage the intended target [13,32]. This concept of standoff distance allows defining the spatial relationship between the location of the target, the location of the physical barriers within the PPS, and the location of the adversary. Thus, it is similar to the concept of "safety distance" or "protection distance" in the safety domain [33]: e.g., Gouller [34] reports safety distances for the storage of liquefied gases, Laska [35] for hazardous pressurized gas storage, Healy [36], Jarret [37], and Mercx et al. [38] for explosives, and Schonbucher et al. [39] for flammable liquids potentially originating pool fires.

A study carried out by Landucci et al. [31] provides values of standoff distances for credible attacks with home-made explosives by using a TNT equivalence model as vulnerability model to assess the damage caused by overpressure with distance from the target. Dusso et al. [40] investigate protection distances for fire-induced adverse scenarios inside chemical and pharmaceutical warehouses by using simplified vulnerability models for fire effects in enclosed areas. Standoff distances for high-explosive munitions (e.g., detonation of a single 105 mm projectile) are provided by Qin and co-authors [41]: however, in this case, humans are considered as the targets of the shooting attacks and thus the proposed standoff distances are not applicable in the context of asset integrity and loss prevention in the CPI.

To date, the assessment of standoff distances for shooting attacks to CPI critical assets received scarce attention in the open literature. The lack of suitable damage models for projectile impact on chemical and process equipment hampers the ability to assess the vulnerability to perforation of storage tanks and process vessels accurately. Thus, the implementation of adequate protective measures to mitigate the potential consequences of shooting attacks is not straightforward in the current industrial practice. Models providing a quantitative approach to the assessment of the potential impacts of shooting attacks (e.g., extent of damage with respect to distance from the target) would be of vital importance to improve site security. Actually, as stated by Dong and co-workers [42], optimizing the vulnerability level of a facility plays a crucial role in preventing and controlling security incidents.

Most of the available studies on the damage caused by projectile impact focus on target materials as armour steel [43,44] and titanium, aluminium, and steel alloys [45–47], that have relevant differences from the steel alloys typically used as construction material for the shells of atmospheric and pressurized storage tanks. The only studies devoted to the analysis of damage of CPI storage and process equipment caused by projectile impact refer to fragments originated by equipment failure in

domino events [48–51]. However, these fragments have shape, mass, and velocity very different from light weapon projectiles used in shooting attacks [52,53].

In a recent study [54], the most reliable projectile perforation models for both soft-core and hard-core light projectiles impacting typical construction materials of atmospheric and pressurized storage tanks were identified through a validation process based on experimental data and statistical performance indicators. Based on these results, the present study aims at filling the gap evidenced above, providing a scientifically sound approach to the quantitative vulnerability assessment of shooting threats. The calculation of standoff distances for shooting attacks carried out using handguns and rifles to atmospheric and pressurized cylindrical storage tanks used for the bulk storage of hazardous chemicals is addressed. A novel specific modelling approach was developed, based on the combination of validated projectile perforation models [54] with an exterior ballistics model consisting in a well-accepted and experimentally validated projectile flight model [55–57]. The model was used to obtain baseline values of standoff distances for a representative set of standardized light weapon projectiles for both atmospheric and pressurized storage tanks taken as targets in the present analysis. The uncertainties deriving from the shooting precision of the different weapons considered was investigated by a Monte Carlo analysis addressing the effect of the shooting angle on standoff distances. A case study addressing the storage section of a chemical plant (flammable liquid stored inside the tanks) is presented to demonstrate the potential use of the baseline standoff distances obtained by the proposed novel approach in supporting SVA/SRA studies and in improving site vulnerability level and security (e.g., attack detection, emergency response, and mitigation plans).

2. Methodology

2.1. Overview

An original approach was developed for the calculation of baseline values of standoff distances (SOD) for shooting attacks to atmospheric and pressurized storage tanks containing hazardous materials (e.g., flammable and/or toxic materials) in the CPI. The workflow of the method is shown in Fig 1. The method is composed of three main steps: setup of the analysis (Step 1), calculation of the ballistic limit velocities (Step 2), and calculation of the standoff distances (Step 3). The detailed description of each step is provided in the following.

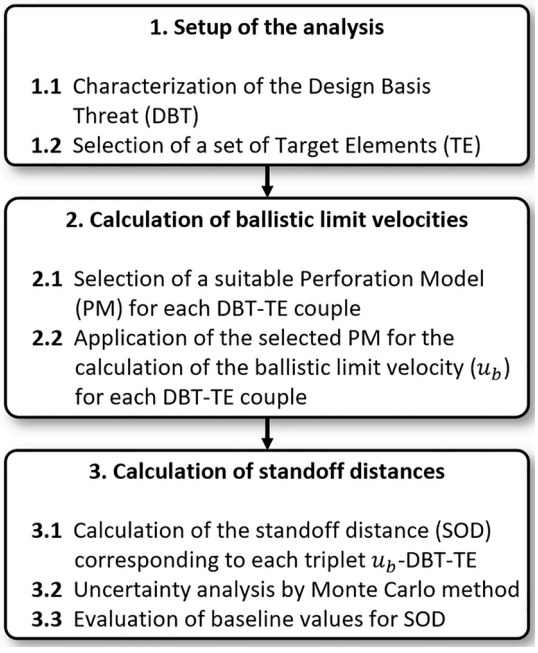

Fig. 1. Workflow of the method developed in the present study to calculate baseline standoff distances.

2.2. Design basis threat and target elements (Step 1)

The first step of the method developed in the present study concerns the definition of the scope of the analysis. This consists in the characterization of the Design Basis Threat (DBT, Step 1.1 in Fig 1) and in the selection of the Target Elements (TE, Step 1.2 in Fig 1).

2.2.1. The design basis threat

The concept of Design Basis Threat (DBT) is frequently adopted in the context of SVA/SRA [18,20,32], consisting in the characterization of the adversary in terms of its characteristics (skills and motivations) and capabilities. Given the scope and aim of the present study, the DBT is here restricted to shooting attacks with light weapons such as handguns and rifles. Thus, characterizing the DBT requires selecting a set of projectiles which may be fired by an adversary (see Fig 2). A highly skilled and well-motivated adversary was assumed (worst-case scenario).

There are many types of projectiles available [58]. A first classification introduced in the literature considers the material used to manufacture the projectile core [59,60]: lead or mild steel are typically used for soft-core projectiles (SC, commonly referred to as “ball” rounds), while hardened steel or tungsten carbide are used in case of hard-core projectiles (HC, commonly referred to as “armour-piercing” (AP) projectiles). Clearly, SC and HC projectiles have different perforation capabilities: the hard-core projectiles are generally characterized by relatively higher kinetic energy densities (i.e., the kinetic energy divided by the cross-sectional area offered by the projectile) and higher hardness values of the cores, resulting in higher perforation depths on the target [59].

Projectiles can be also classified on the basis of their geometrical shape (see Fig 3) [58,61]: pointed (P) conical or ogival projectiles, projectiles with a round nose (RN), projectiles with a flat nose (FN) also referred to as “blunt” projectiles, and spherical projectiles (S).

In the present study, a reference set of projectiles was considered, retrieved from the standards EN 1522 [62] and EN 1063 [61]. Both standards classify target resistance to perforation according to protection classes (FB codes) which are in turn associated to different categories of projectiles.

Five reference projectiles were selected in the DBT, each corresponding to a different protection class in EN 1522 and EN 1063. Table 1 reports the relevant information of each reference projectile selected. The code name used in the table (FB code) refers to the original specification in EN 1522 and EN 1063. It shall be noted that in case of FB7 projectiles, data in Table 1 refer to the core diameter and mass, as jacket and lead cap have minor influence on penetration by armour piercing projectiles as demonstrated by the studies of Børvik et al. [60], Chen et al. [63], and Hazell [59].

These projectiles are small-medium calibre bullets that find extensive use in civilian self-defence and recreational shooting (e.g., target practice and competitive shooting sports), as well as in military and law enforcement scenarios (e.g., combat, patrol, and close-quarters engagements) [64]. Therefore, the five reference projectiles selected allow representing a wide set of projectiles with different performances, both for handguns (FB2 and FB4) and for rifles (FB5, FB6, and FB7). Larger calibre bullets have been considered out of the scope of the present analysis, due to a much more reduced field of application (e.g., anti-materiel roles, long-range sniping, heavy machine guns). In fact, these projectiles due to their increased power and penetration capabilities with respect to standard small-medium projectiles, need specific requirements for their deployment. Adversaries with high to critical capabilities, as defined by the CCPS SVA [18], may not be available.

The typical values suggested in the literature for accuracy of hand-

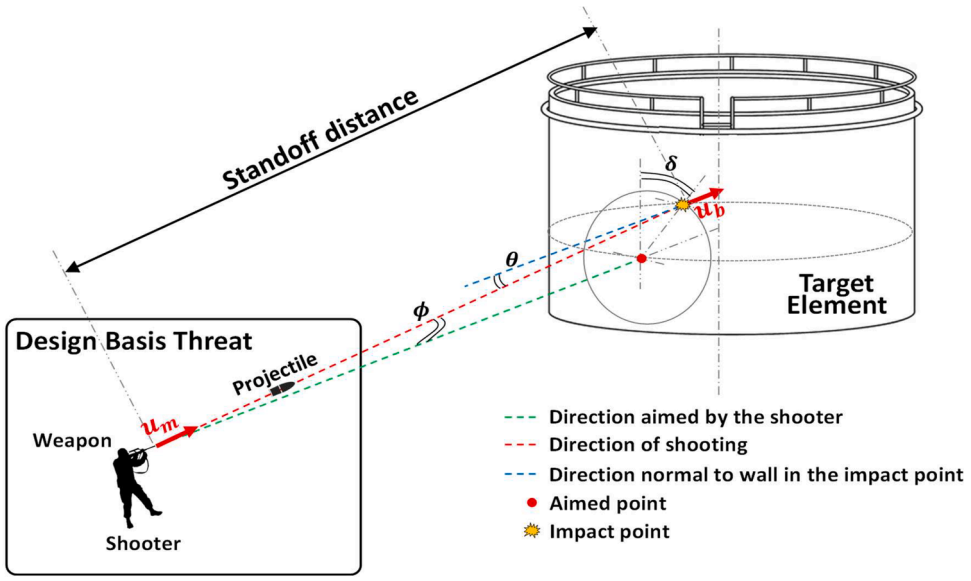

Fig. 2. Schematization of the shooting attack and its geometry: Design Basis Threat (DBT), Target Element (TE), and standoff distance. u_m: muzzle velocity; u_b: ballistic limit velocity; ϕ: initial offset angle; θ: impact angle; δ: initial azimuthal angle. Further details on the definition of variables are reported in the Nomenclature section.

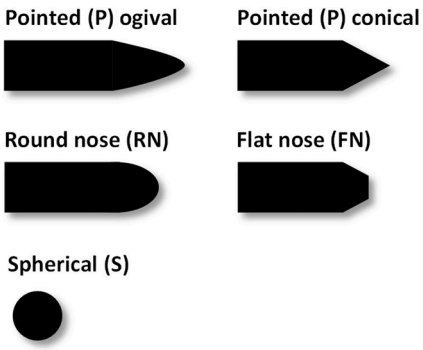

Fig. 3. Classification of projectiles with respect to shape according to [58,61].

guns and rifles [65–67] were considered for the reference initial offset angle (ϕ_r). These angles are usually expressed in the form of MOA (Minute Of Angle): one MOA is 1/60th of a sexagesimal degree of arc and spreads about 1.047" per 100 yards [68].

2.2.2. The target elements

The Target Elements (TE) are the objects that are aimed by the shooter in the context of a shooting attack. The vulnerability to perforation of a TE depends primarily on the shape and material composition.

The target shape plays an important role in determining the target resistance to perforation: in fact, objects with the same thickness, but different shapes (e.g., flat plates, curved surfaces, or angled structures) may have different ballistic limit velocities, and in turn different values of standoff distance.

In the chemical and process industry, the tanks used for the bulk storage of liquid are mostly cylindrical or spherical [33]. Cylindrical equipment finds more extensive use in industrial sites due to the simpler construction and installation, to the possibility of mounding, and to the reduced visual impact [69]. On the other hand, spherical storage tanks are limited to specialized applications such as high-capacity pressurized vessels and cryo-compressed storage (e.g., liquid hydrogen storage). Therefore, due to the much more limited field of application and to the less frequent use, spherical vessels are not further considered in the present analysis. Moreover, as discussed in Section 3.2, the results obtained in the present study for cylindrical vessels can be used as conservative baseline standoff distances for spherical tanks.

Two sets of reference cylindrical vessels were considered as TEs: Table 2 reports the set of atmospheric vertical cylindrical storage vessels (a-codes), while Table 3 shows the set of pressurized horizontal cylindrical storage vessels (p-codes) considered. Design data of the tanks were derived from a former study by Cozzani et al. [70]. The tables also report the main design parameters for each equipment item such as design pressure, volume, diameter, and shell thickness. The latter parameter, which plays a key role in the context of material perforation, shows a large variability within practical applications since it depends on tank design (e.g., design pressure, diameter, height, corrosion allowance). High diameter atmospheric vessels (e.g., codes from a.5 to a.10 in Table 2) are characterized by a decreasing shell thickness with height to account for the different hydrostatic load. The thickness values reported in the original source for the lower section of the shell were

Table 1
Selected reference projectiles from [62,61]. RN=Round nose, SC=Soft-core (lead), FN=Flat nose, *P*=Pointed, SCP1=Soft-core (lead) with steel penetrator, HC=Hard-core (steel, hardness more than 63 HRC). *FB7 data reported refer to the hard-core of the projectile.

Protection Class	Type of weapon	Reference projectile	Projectile type	d (mm)	m (g)	u_m (m/s)	ϕ_r (MOA)
FB2	Handgun	9 mm Luger	RN/SC	9	8	400	20
FB4	Handgun	44 Rem. Mag.	FN/SC	11	15.6	440	20
FB5	Rifle	5.56×45	PB/SC	5.56	4	950	1
FB6	Rifle	7.62×51	P/SC	7.62	9.5	830	1
FB7	Rifle	7.62×51	FP/HC	6.06*	3.7*	820	1

d : projectile diameter; m : projectile mass; u_m : muzzle velocity; ϕ_r: reference initial offset angle.

Table 2
Set of atmospheric vertical cylindrical storage vessels selected in the present study (adapted from [70]).

ID	V (m^3)	D (mm)	t (mm)	t_d (mm)	t_{eff} (mm)
a.1	25	2700	5	0.3	4.7
a.2	100	4400	5	0.7	4.3
a.3	250	6700	5	1.2	3.8
a.4	750	10,500	7	2.3	4.7
a.5	1000	15,000	9	2.1	6.9
a.6	2500	16,000	13	4.9	8.1
a.7	5200	25,000	19	6.5	12.5
a.8	10,000	30,000	20.5	10.4	10.1
a.9	13,390	34,130	20	12.1	7.9
a.10	17,480	39,000	23	13.8	9.2

V : vessel volume; D : vessel diameter; t : target actual thickness; t_d: target thickness by design; t_{eff}: target effective thickness.

Table 3
Set of pressurized horizontal cylindrical storage vessels selected in the present study (adapted from [70]).

ID	P_d (MPa)	V (m^3)	D (mm)	t (mm)	t_d (mm)	t_{eff} (mm)
p.1	1.5	5	1000	11	3.2	7.8
p.2	1.5	10	1200	11	3.8	7.2
p.3	1.5	20	1500	12	4.8	7.2
p.4	1.5	25	1700	15	5.4	9.6
p.5	1.5	50	2100	17	6.7	10.3
p.6	1.5	100	2800	18	8.9	9.1
p.7	1.5	250	3800	24	12.0	12.0
p.8	2	5	1000	14	4.2	9.8
p.9	2	10	1200	14	5.1	8.9
p.10	2	20	1500	16	6.3	9.7
p.11	2	25	1700	20	7.2	12.8
p.12	2	50	2100	23	8.9	14.1
p.13	2	100	2800	24	11.8	12.2
p.14	2	250	3800	32	16.1	15.9
p.15	2.5	5	1000	17	5.3	11.7
p.16	2.5	10	1200	17	6.3	10.7
p.17	2.5	20	1500	20	7.9	12.1
p.18	2.5	25	1700	24	9.0	15.0
p.19	2.5	50	2100	29	11.1	17.9
p.20	2.5	100	2800	30	14.8	15.2
p.21	2.5	250	3800	40	20.1	19.9

V : vessel volume; D : vessel diameter; t : target actual thickness; t_d: target thickness by design; t_{eff}: target effective thickness.

considered. No corrosion allowance was accounted (i.e., the thickness was considered equal to corroded thickness). In the present study, a cylindrical geometry was assumed for the TE, thus neglecting the actual shape of the heads of pressurized vessels due to their limited size with respect to the cylindrical shell of the vessel.

With respect to the properties of the construction material of the selected TEs, the steel with the lowest strength (coded as A 285M-C steel) from the list present in standard API 650 [71] and Section VIII of ASME Boiler & Pressure Vessel Code [72] was considered for both the atmospheric and pressurized storage vessels. This choice yields safe-side results (overestimation of ballistic limit velocity compared to other steel materials). However, the differences on ballistic limit velocity considering other materials are expected to be small. A previous study [54] evidenced that the effect of target material on u_b is negligible, especially for SC projectiles.

The mechanical properties (ρ_t=7850 kg/m^3, E=200 GPa, σ_T=205 MPa, σ_R=380 MPa) of the considered steel were retrieved from standard API 650 [72]. The hardness (BHN_t=110) was evaluated using the correlation reported in Callister and Rethwisch [73], while other parameters required in the application of the projectile perforation models (i.e., G=80 GPa, τ_s=220 MPa, K=158 GPa, ν=0.3) were taken from Zukas [74].

2.3. Ballistic limit velocity and projectile perforation models (Step 2)

The second step (Step 2) of the method developed in the present study (see Fig 1) is devoted to the calculation of the ballistic limit velocity (u_b), which is required for the further calculation of standoff distances in Step 3.

The ballistic limit velocity is defined as the minimum projectile velocity required to perforate a target at normal incidence [75], and is usually estimated using projectile Perforation Models (PMs). Therefore, based on the characteristics of the selected DBT and TEs (from Step 1), suitable PMs were selected (Step 2.1 in Fig 1) and used to calculate u_b for each DBT-TE couple (Step 2.2 in Fig 1).

In general, a PM is a function of many parameters of both the projectile and the target:

$$u_b = f\left(d,\ m,\ t_{\max},\ \theta,\ \rho_p,\ \rho_t,\ \sigma_T,\ Y,\ BHN_p,\ BHN_t,\ E,\ f,\ \tau_S,\ K,\ G,\ \alpha,\ \nu,\ C_n,\ C_v\right) \quad (1)$$

where $u_{b,n}$ is the normal component of the ballistic limit velocity, and the model parameters are: projectile diameter (d), projectile mass (m), target maximum perforated thickness (t_{max}), impact angle (θ), projectile density (ρ_p), target density (ρ_t), target yield stress (σ_T), target dynamic yield stress (Y), projectile Brinell's hardness number (BHN_p), target Brinell's hardness number (BHN_t), target Young modulus (E), friction coefficient (f) between the target and the projectile, target static shear strength (τ_S), target bulk modulus (K), target shear modulus (G), half-angle of conical nose of the projectile (α), Poisson ratio (υ), and projectile model-specific parameters (C_n, C_v).

The most reliable projectile perforation models for both soft-core and hard-core light projectiles impacting typical construction materials of atmospheric and pressurized industrial storage tanks were identified in a recent study [54]. In the study, 17 projectile perforation models (empirical, analytical, and numerical PMs) were retrieved from open literature and validated using a dataset obtained from experimental perforation tests.

According to the findings obtained in the previous study [54], the *Modified De Marre* model [59,76] and the *Recht* model [45,74] resulted to be the best models fitting the experimental data and thus were selected to cover the behaviour of SC and HC projectiles repectively. These models provide the maximum perforated thickness (t_{max}) for a flat steel target sheet with no stress applied. They were developed considering u_b direction as perpendicular to the target surface (normal incidence). Since, in general, the direction of projectile velocity may not be perpendicular to the shell of the equipment at the point of impact, a simple trigonometric relation is proposed to correlate the ballistic limit velocity at the impact point (u_b) with its normal component ($u_{b,\ n}$) [74]:

$$u_b = \frac{u_{b,n}}{\cos\theta} \tag{2}$$

where θ is the impact angle (polar angle in a spherical coordinate system with the impact point as origin and the normal to the target wall as polar axis).

The *Modified De Marre* model was selected for the calculation of $u_{b,n}$ (m/s) in case of impact of the selected TEs with a SC projectile (i.e., FB2, FB4, FB5, and FB6 projectiles listed in Table 1). The model equation, which is based on empirical characterization of test data, is the following:

$$t_{max} = 5.42 \times 10^{-6} u_{b,n}^{4/3} m^{1/3} \tag{3}$$

where m is the mass of the projectile (kg) and t_{max} is the maximum perforated thickness (m).

The *Recht* model was selected for the calculation of $u_{b,n}$ (m/s) in case of impact of the selected TEs with a HC projectile (i.e., FB7 projectiles in Table 1). This PM was developed for non-deformable pointed projectiles (see Fig 3) penetrating in a semi-infinite slab, and it is based on the following equations:

$$t_{max} = \frac{4\left(\frac{m}{\pi d^2}\right)}{C_n b}\left[u_{b,n} - \frac{a}{b}\ln\left(\frac{a + b u_b}{a}\right)\right] \tag{4}$$

$$a = 2\tau_s \ln(2Z_m)\cdot\left(1 + \frac{f}{\tan\alpha}\right) \tag{5}$$

$$b = C_v\sqrt{K\rho_t}\left(1 + \frac{f}{\tan\alpha}\right)\sin\alpha \tag{6}$$

$$Z_m = \frac{E}{\sigma_T}\left(1 + 2\frac{E}{\sigma_T}\right)^{-0.5} \tag{7}$$

where m and d are respectively the mass (kg) and the diameter (m) of the projectile core, C_n and C_v are specific parameters of the projectile (equal to 0.62 and 0.25 respectively [74]), α is the half-angle of conical nose (equal to 23.5 for standard ogives [74]), σ_T and E are the static yield strength (Pa) and the Young modulus (Pa) of the target material, f is the dynamic friction coefficient (equal to 0.01 for metal on metal [45]), K and τ_s are the bulk modulus (Pa) and the static shear strength (Pa) of the target (estimated from data reported in [74]).

It is important to stress that all the thickness values considered and calculated in the present analysis are intended as corroded thicknesses (i.e., initial thickness subtracted of the corrosion allowance). This aims to provide a safe-side evaluation of the ballistic limit velocities as the actual attack may occur at any possible moment of the tank life. Moreover, in most applications the corrosion phenomena are superficial processes, not affecting the mechanical properties of the bulk material of the tank walls.

2.3.1. Target effective thickness

An important element that shall be taken into account in the calculation of the ballistic limit velocity for a given target material and projectile is the stress applied to the wall of the target elements (cylindrical steel vessels in the present analysis): this aspect is not addressed by the selected PMs [54]. In case of atmospheric vessels, the stress is mainly generated by the hydrostatic load (liquid hold-up contained inside), while in the case of pressurized vessels it is generated by the internal design pressure.

The use of the actual thickness (t) of the target element in Eqs. (3) and (4) may lead to an overestimation of the ballistic limit velocity needed for perforation (and in turn to an underestimation of the standoff distance, which is not conservative) as the formation of a hole is facilitated by the tensile stress present in the wall of the vessel. This is expected to be a critical issue, especially in the case of high internal pressures.

To overcome this limitation, in the present study it is pragmatically assumed that successful perforation occurs when the projectile penetrates the target wall until the remaining non-penetrated thickness is equal or lower than the minimum thickness required to resist the mechanical stress (t_d) generated by the internal design pressure and/or by the design hydrostatic load. In other words, perforation is considered to occur if the target maximum perforated thickness (t_{max}) calculated with the PM exceeds the target effective thickness (t_{eff}) defined as:

$$t_{eff} = t - t_d \tag{8}$$

where t is the actual shell thickness and t_d is the shell design thickness value required to withstand the internal design pressure and/or the design hydrostatic load. The shell design thickness (t_d) for pressurized horizontal cylindrical vessels is calculated applying the Von Mises criterion considering a planar stress state [77]. In particular, it is calculated using the following equation:

$$t_d = \frac{\sqrt{3}P_d D}{4\sigma_e} \tag{9}$$

where σ_e is the Von Mises equivalent stress (MPa) equal to $\sqrt{3}\tau_s$ in case of pure shear, P_d is the design internal pressure (MPa), and D is the vessel diameter (m).

Differently, in the case of atmospheric vertical cylindrical storage vessels, t_d is calculated considering the hydrostatic load according to the equation reported in standard API 650 [71] for hydrostatic test condition:

$$t_d = \left(1.06 - \frac{0.0696D}{H}\sqrt{\frac{H}{\sigma_T}}\right)\cdot\frac{4.9HD}{\sigma_T} \tag{10}$$

where D is the vessel diameter (m), H is maximum design liquid level (m), σ_T is the target yield stress (MPa).

Values of t, t_d, and t_{eff} for each reference vessel considered in the present study as TE are reported in Tables 2 and 3, that are, according to the assumption on corrosion issue adopted in the present study, corroded thicknesses (the corrosion allowance is not accounted in the thickness value).

2.4. Calculation of standoff distances (Step 3)

The last step (Step 3) of the method developed in the present study (see Fig 1) is devoted to the calculation of standoff distances (SOD).

According to Landucci et al. [31], the SOD is defined as the minimum distance between the location of the adversary and that of the target asset (the TE) that will not cause any significant damage to the TE. In the case of concern, the SOD is therefore the downrange distance (d_r, i.e., the horizontal distance travelled by the projectile from the muzzle of the weapon to the TE) corresponding to an impact velocity equal to the ballistic limit velocity (see the graphical representation of Fig 2).

2.4.1. Calculation of maximum standoff distances

Calculation of standoff distances requires the modelling of the projectile flight to evaluate the decay of the horizontal component of the projectile velocity as a function of the downrange distance. To this purpose, exterior ballistics models [55] were adopted to calculated SOD for each triplet u_b-DBT-TE (Step 3.1 in Fig 1).

In general terms:

$$SOD = f(u_b,\ u_m,\ C,\ G) \tag{11}$$

where u_b is the ballistic limit velocity, u_m is the muzzle velocity, C and G are parameters of the exterior ballistics model (i.e., the ballistic coefficient and the projectile drag function respectively).

Exterior ballistics calculations require the solution of differential equations describing the projectile trajectory. These are commonly solved with approaches based on simplified assumptions such as constant atmospheric density and departure angle less than 15° [55]. In the present study, the Siacci method is adopted to model the exterior ballistics. The method is of widespread use throughout US sporting arms and ammunition industry and its accuracy in performing flat-fire trajectory calculations is sufficient for nearly all practical purposes [55]. An experimental validation of the method was performed by Zhai and co-workers [56] and by Kapoor [57] that used the model to fit experimental data of distance and velocity of projectile in flight with good results. The Siacci method is summarized in Appendix A, while further details are reported in the literature [55].

A first estimation of the standoff distance is obtained assuming the perpendicular impact of the projectile on the wall of the target (i.e., impact angle $\theta = 0$ in eq. (2), and thus $u_b = u_{b,n}$). This corresponds to the case of a shooter aiming at the target from a direction perpendicular to the vessel axis with no initial offset angle ($\phi = 0$). Fig 4 shows exemplifications of this geometry in case of vertical and horizontal vessel targets as TEs. Any other direction of the aim of the shooter (e.g., shooter aiming off-axis or axis of the vessel non-perpendicular to the direction of aim) increases the angle of impact of the projectile ($\theta > 0$) in comparison to the considered case, reducing the kinetic energy available for penetration (eq. (2)). Hence, the assumption considered here defines the worst case in terms of available projectile velocity and standoff distance, leading to conservative (safe-side) results compared to other assumptions, and it is therefore of interest in the context of the present study aimed at providing baseline standoff distances.

The value of standoff distance calculated in this case (referred in the following as "maximum standoff distance", SOD_0) is representative of a worst-case scenario in which shooting is unaffected by external factors that may reduce its value (e.g., ability of the shooter, flaws of the weapon, wind, etc.). SOD_0 is thus the maximum expected value for standoff distance, beyond which inherent safety is achieved (no possibility of damage).

2.4.2. Uncertainty analysis by Monte Carlo method

In order to assess the effect of the uncertainty on the standoff distance (SOD) due to the inevitable factors that influence it even under the worst credible conditions considered above, a Monte Carlo analysis was applied (Step 3.2 in Fig. 1). Reduction of SOD due to factors such as different angles of aim on the vessel axis, limitations in the ability of the shooter, random flaws of the weapon, and adverse weather conditions were conservatively neglected as they are external factors, with a large variability from case to case and therefore deemed unsuitable for the definition of standoff distances of general application.

On the contrary, even in case of highly skilled shooter and favourable conditions, an inherent error in the accuracy of the shooter-weapon system exists in all cases and can not be overlooked. This inherent error leads to an impact point on the target element that may differ from the one aimed at by the shooter (offset). This may be schematized by the definition of a system of polar coordinates centred on the shooter (Fig 2): an initial offset angle (ϕ), which is the polar angle of the impact point relative to the polar axis identified by the point aimed by the shooter, and the initial azimuthal angle (δ), which is the azimuthal angle of the impact point relative to the reference direction identified by the vessel axis. Reference values for the initial offset angle (ϕ_r) were defined in Step 1.1 for each projectile class considered (see Section 2.2). Initial azimuthal angle (δ) can be reasonably assumed to have no preferential direction (equally probable for all the possible values along a circle).

Even maintaining the other safe-side assumptions introduced in Section 2.4.1 on the direction aimed by the shooter, an initial offset angle (ϕ) higher than 0 results in an impact angle (θ) on the target element (see Fig 2) higher than zero (i.e., a non-perpendicular impact) or, in extreme cases, in missing the target. For this reason, the effect of ϕ

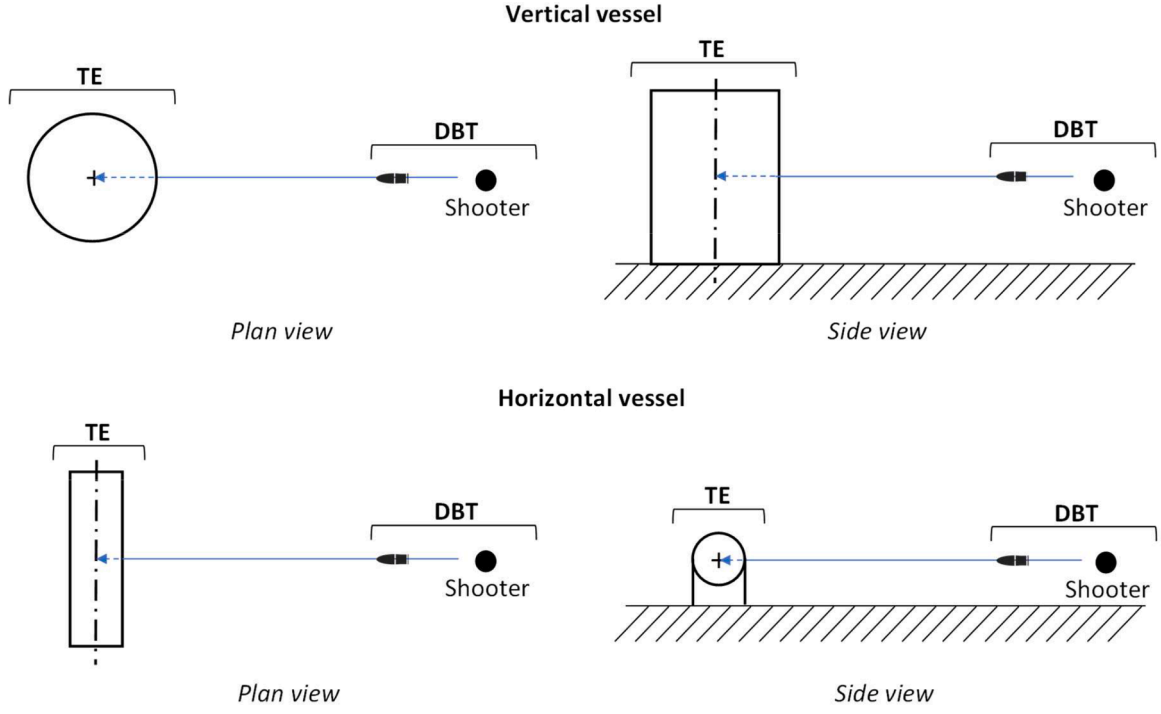

Fig. 4. Geometry assumed for the shooting attack (impact at normal incidence). DBT: Design Basis Threat; TE: Target Element.

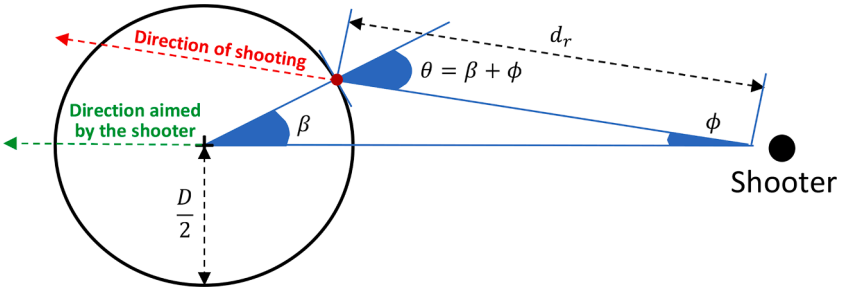

Fig. 5. Definition of angles in case of an initial offset angle on the plane perpendicular to the target axis ($\boldsymbol{\delta} = \frac{\pi}{2}$). $\boldsymbol{D}$: target vessel diameter; $\boldsymbol{\phi}$: initial offset angle; $\boldsymbol{\beta}$: azimuthal angle of the impact point on the vessel; $\boldsymbol{\theta}$: impact angle; $\boldsymbol{d_r}$: downrange distance. Further details on the definition of variables are reported in the Nomenclature section.

on SOD is more pronounced for target elements with a low diameter.

The offset angle ϕ results in the maximum effect on the ballistic limit velocity, and in turn on reducing the standoff distance, if considered on the plane perpendicular to the axis of the cylindrical target (i.e., an horizontal offset angle in case of vertical cylindrical targets and a vertical offset angle in case of horizontal cylindrical targets) as the effect of curvature on the impact angle θ is the greatest in this case. Hence, this direction for ϕ, defined by $\delta = \frac{\pi}{2}$, is considered in the following Monte Carlo analysis. Fig 5 shows the definition of the angles in this case.

Under this assumption, the impact angle (θ in Fig 5), the azimuthal angle of the impact point on the vessel (β in Fig 5), and the initial offset angle on the plane perpendicular to the vessel axis (ϕ in Fig 5) are geometrically correlated by Eqs. (10) and (11), as follows:

$$sen(\beta) = d_r \cdot sen(\phi) \cdot 2/D \tag{12}$$

$$\theta = \beta + \phi \tag{13}$$

where d_r is the downrange distance and D is the vessel diameter.

The combined solution of the system of Eqs. (1), (2), (9), (10), and (11) results in the estimation of the standoff distance (SOD) for each value of offset angle. In particular, given the reference offset angles (ϕ_r) defined in Section 2.2, a normal distribution with central value 0 and standard deviation $\phi_r/2$ was assumed as a probability density function for the initial offset angle ϕ. The Monte Carlo analysis was applied to calculate a cumulative probability density function for the target effective thickness that can be perforated. Further details on the simulations are reported in Appendix B.

Considering the cumulative probability density function obtained, standoff distances were calculated as a function of the probability of exceedance (PE) of vessel perforation. PE is defined as the probability that a specific value of the target effective thickness will be exceeded: e.g., a 10% probability of exceedance (PE_{10}) is equal to the value of the population cumulative probability density function where 90% of the cumulative probability density is below the value and 10% is above.

In the present study, the standoff distances corresponding to probabilities of exceedance of 1%, 5%, 10%, 30%, and 50% were calculated (defined respectively as SOD_1, SOD_5, SOD_{10}, SOD_{30}, and SOD_{50}). For instance, given a target vessel and a projectile, SOD_{10} refers to the value of standoff distance corresponding to PE_{10}, for which there is thus a 10% probability of vessel perforation by shooting. Clearly enough, the standoff distance related to a probability of exceedance of 0% is the maximum standoff distance, i.e., SOD_0.

2.4.3. Evaluation of baseline values of standoff distance

In this step (Step 3.3 in Fig 1) baseline standoff distances were evaluated from the results obtained from Step 3.1 (worst-case or deterministic calculation of SODs) and Step 3.2 (probabilistic calculation of SODs based on probability of exceedance). In particular a safe-side criterion was followed, considering as baseline standoff distances the highest standoff distance from those calculated for each considered set of TEs (i.e., atmospheric and pressurized storage vessels).

These values are proposed as baseline standoff distances to be used in the context of SVA/SRA studies to assess the shooting threat to tanks storing hazardous materials.

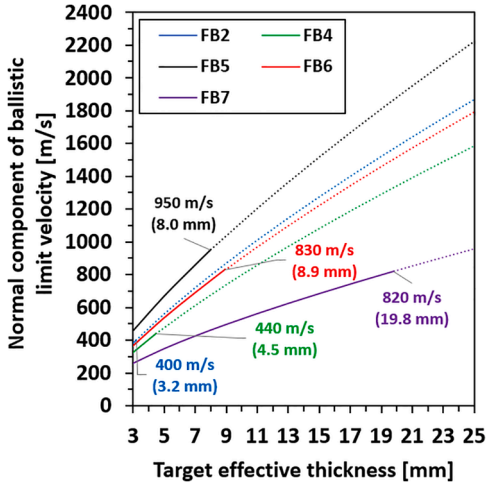

Fig. 6. Normal component of the ballistic limit velocity (m/s) vs target effective thickness (mm) calculated for FB2, FB4, FB5, FB6, and FB7 projectiles (FB-codes defined in Table 1). TE made of Steel A 285 M – C. Muzzle velocities (m/s) and corresponding maximum perforable thicknesses (mm) are reported for each FB class. Continuous lines: values below muzzle velocity. Dotted lines: values above muzzle velocity.

3. Results and discussion

3.1. Ballistic limit velocity vs effective thickness of the target elements

The projectile perforation models (PM) described in Section 2.3 were applied to calculate the normal component of the ballistic limit velocity ($u_{b,n}$) for each standardized projectile selected in the DBT (see Table 1) considering different values of target effective thickness (t_{eff}). The results of the calculations are shown in Fig 6. For each projectile, the higher the thickness of the TE, the higher the ballistic limit velocity required for perforation (the curves are monotonically increasing). Each curve in the figure is represented as a continuous line till the point in

which the normal component of the ballistic limit velocity matches the muzzle velocity (u_m, also reported in Fig 6). This point represents the maximum velocity at which a projectile can impact the target element (i.e., when the muzzle of the firearm is next to the external surface of the TE). Perforation is no longer possible if it requires a $u_{b,n}$ higher than u_m (dotted part of curves in Fig 6): thus, a limit is present in the effective thickness that can be perforated by each projectile. An inherently safe region may this be defined, including thickness values higher than the thickness corresponding to the muzzle velocity for each FB class, i.e., the maximum perforable thickness [78]. The calculated maximum perforable thickness values for each reference projectile considered in the DBT are reported in Fig 6 together with the corresponding muzzle velocity.

These results highlight a relevant variation in the perforable thickness between handgun projectiles (FB2 and FB4 in Table 1) and rifle projectiles (FB5, FB6, and FB7 in Table 1). In fact, an adversary who shoots with a handgun that uses FB2 and FB4 projectiles will not be able to perforate TEs with an effective thickness higher than 4.5 mm, while, on the other hand, greater thicknesses can be perforated using rifles (maximum perforated thickness equal to 19.8 mm in case of FB7 projectiles). This proves that a higher level of threat may be associated to shooting attacks involving rifles with respect to shooting attacks involving handguns. This aspect will be better addressed in the discussion of standoff distances (Section 3.2) and in the case study (Section 4).

Overall, the curves reported in Fig 6 can be used to easily assess the minimum value of the normal component of the ballistic limit velocity for which perforation is possible in case of the atmospheric and pressurized TE storage vessels reported respectively in Tables 2 and 3.

The results are reported in Table 5 and Table 6 respectively (see Section 3.3).

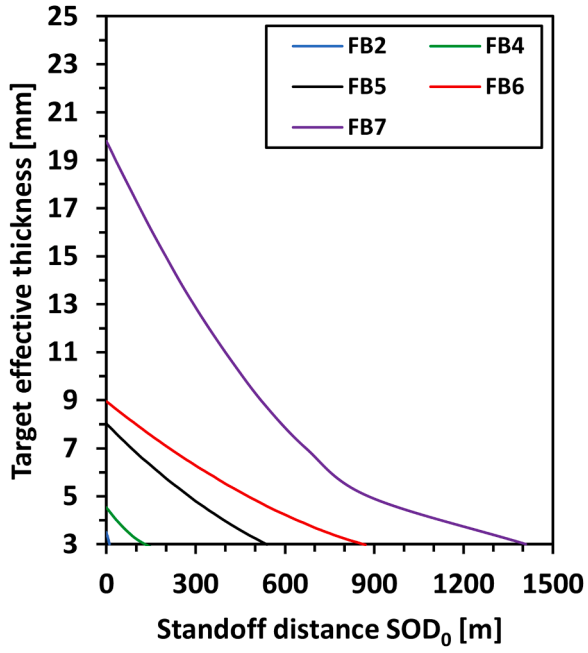

Fig. 7. Maximum standoff distance (SOD_0) for normal impact (m) vs. target effective thickness (mm) calculated for FB2, FB4, FB5, FB6, and FB7 projectiles (FB-codes defined in Table 1). TE made of Steel A 285 M – C.

3.2. Standoff distances vs effective thickness of the target elements

Fig 7 shows the maximum standoff distance (SOD_0) calculated by the method described in Appendix A. As expected, a clear distinction is present in the figure between the maximum standoff distances obtained for handgun projectiles (FB2 and FB4 in Table 1) and those obtained for rifle projectiles (FB5, FB6, and FB7 in Table 1). In fact, taking as an example a target effective thickness of 3 mm, the maximum standoff distance is almost four times higher moving from FB2 (SOD_0 equal to 10 m) and FB4 (SOD_0 equal to 131 m) projectiles to FB5 (SOD_0 equal to 540 m) projectiles, or even more in case of FB6 and FB7 projectiles (SOD_0 equal to 870 m and 1409 m respectively). Similar trends are observed for all the other values of target effective thickness considered.

These results support specific choices in the design of passive protection barriers within the Physical Protection System (PPS) and in the definition of internal and external response plans for chemical and process plants (see Section 4). For example, in case of effective shell thickness equal to 11 mm, which is typical of higher diameter atmospheric storage tanks or of horizontal pressurized storage vessels (e.g., see the values reported in Tables 2 and 3), a standoff distance of about 400 m is calculated considering FB7 projectiles. Shooters may thus be able to successfully perforate such targets even if they are positioned outside the plant boundaries. Therefore, external security arrangements are required to increase the probability of detection and of interruption of the attack (e.g., clearance areas and/or external Closed-Circuit Television (CCTV) system).

In order to investigate the effect of the offset angle on the standoff distance, Monte Carlo simulations were carried out (details in Appendix B). Since a smaller TE diameter (D) corresponds to a greater curvature, the minimum value amongst the vessel diameters considered as TEs in the present study (see Section 2.2) was used in the simulation. The simulations were thus carried out considering a vessel diameter equal to 1 m, for which the effect of the offset angle is the most relevant. Table 4 shows the results of Monte Carlo simulation for FB4 projectiles (worst-case projectile scenario for handguns). Fig B.2 in Appendix B reports the results obtained for the other projectile classes (FB2 to FB7).

In Table 4 the maximum standoff distance (SOD_0) and those corresponding to a probability of exceedance (PE) of 1% (SOD_1), 5% (SOD_5), 10% (SOD_{10}), 30% (SOD_{30}), and 50% (SOD_{50}) are reported with respect to the target effective thickness. It can be observed that, when considering a constant probability of exceedance different from 0, the percentage variation of the standoff distance with respect to SOD_0 increases with increasing SOD. This is due to the fact that the angle of view, for which successful penetrations are possible (i.e., wall and projectile trajectory are almost perpendicular, leading to higher values of $u_{b,n}$ for a given u_b), becomes smaller with distance: with increasing downrange distance, the portion of the initial offset angle distribution where a complete penetration (i.e., perforation) takes place becomes gradually smaller.

Table 4
Results of Monte Carlo simulations for FB4 projectiles considering target diameter (D) of 1 m and initial offset angle (ϕ) of 20 MOA.

t_eff (mm)	SOD_0 (m)	SOD_1 (m)	SOD_5 (m)	SOD_{10} (m)	SOD_{30} (m)	SOD_{50} (m)
1.5	648	647 (−0.2%)	618 (−4.6%)	544 (−16%)	299 (−54%)	191 (−71%)
2.0	398	397 (−0.1%)	387 (−2.6%)	360 (−9.5%)	233 (−42%)	160 (−60%)
2.5	229	229 (−0.05%)	226 (−1.2%)	218 (−4.9%)	168 (−27%)	126 (−45%)
3.0	132	132 (−0.02%)	131 (−0.5%)	129 (−2.1%)	112 (−15%)	93 (−30%)
3.5	74.5	74.5 (−0.01%)	74.4 (−0.2%)	73.9 (−0.9%)	69.1 (−7.3%)	61.3 (−18%)
4.0	34.4	34.4 (0%)	34.4 (−0.1%)	34.3 (−0.4%)	33.2 (−3.6%)	31.1 (−9.5%)
4.5	2.04	2.04 (0%)	2.04 (−0.07%)	2.03 (−0.3%)	1.98 (−2.7%)	1.88 (−7.7%)

Clearly enough, at a constant t_{eff}, the standoff distance decreases considering larger PEs. For example, in the case of probabilities of exceedance of 30% and 50%, the percentage variation with respect to SOD_0 exceeds 50% for small targets (e.g., a 53.86% increase (SOD_{30}) and a 70.53% increase (SOD_{50}) are calculated for $t_{eff} = 1.5$ mm). On the contrary, the percentage variations are small in case of probability of exceedance of 1% (in the order of 0.1% or even lower). In the case of PE_{10} (i.e., a level of confidence which is one order of magnitude smaller than inherent safety or PE_0), the percentage variation of the standoff distance with respect to SOD_0 is at most 0.21% for the target effective thicknesses of interest for typical industrial storage tanks (from 3.5 mm up). The above considerations for FB4 projectiles can be extended also to all the other classes of projectiles considered in the present study (see Section 2.2) as the differences between SOD_0 and other SODs based on increasing PEs are even smaller in these cases (see Fig B.2 in Appendix B). Given the greater accuracy of rifles (reference offset angle of 1 MOA) compared to handguns (reference offset angle of 20 MOA), the percentage variations of SOD_1, SOD_5, SDO_{10}, SOD_{30}, and SOD_{50} with respect to SOD_0 for FB5, FB6, and FB7 projectiles are negligible (the curves reported in Fig B.2-a, -b, and -c are almost overlapped).

The small difference amongst SOD_0, SOD_1, SOD_5, and SOD_{10} suggests that, in practical cases, the use of a probabilistic risk acceptability criterion (e.g., based on a PE of 1%) does not lead, under the assumptions of the current study, to a relevant reduction in the standoff distances with respect to those obtained by a deterministic criterion based on inherent safety.

It is important to recall that the assumption on the direction of the initial offset angle (i.e., $\delta = \frac{\pi}{2}$ and therefore ϕ on the plane perpendicular to the target axis) does not affect this finding. Actually, the SODs based on probabilistic exceedance criteria referred to a generic direction of ϕ are larger than those obtained considering ϕ limited to a plane perpendicular to the target axis. In fact, considering ϕ on a plane with a generic orientation with respect to the vessel axis leads to a lower impact angle (θ) and therefore to larger SOD values than those estimated under the assumption of ϕ laying on a plane perpendicular to the target axis, since the effect of the target curvature in increasing the impact angle is maximum in the latter case.

The use of the conservative (safe-side) SOD_0 is therefore advised to assess the reference standoff distance in the context of target protection from shooting attacks and vulnerability assessment in SVA/SRA studies [13], as well as in the design of the Physical Protection System of the facility.

It shall be noted that the use of the proposed SODs can be extended as safe-side assumption also to the case of spherical tank targets of the same effective thickness. As a matter of fact, a shooting aimed at the tank centre (i.e., impact angle equal to zero, $\theta = 0$) results in the same SOD_0 calculated for the considered cylindrical vessel case. On the other hand, SODs for $PE > 0$ in spherical tanks are lower than in the case of cylindrical vessels since the effect of the double-curvature of a spherical surface on the increasing impact angle (θ) for shots with non-zero initial offset angle (ϕ) is greater than that of a single-curvature cylindrical surface of the same radius.

3.3. Baseline standoff distances for atmospheric and pressurized storage tanks

The results reported in Section 3.2 were used to develop baseline standoff distances for generic atmospheric and pressurized cylindrical storage vessels. Tables 5 and 6 report the values of ballistic limit velocity (u_b) and maximum standoff distance (SOD_0) respectively for the atmospheric vertical cylindrical and pressurized horizontal cylindrical storage vessels selected as TEs in the present study (see Table 2 and Table 3 respectively). As both the modelling of the projectile in flight (exterior ballistics) and the target damage (projectile perforation) have been validated using experimental datasets (see Iaiani et al. [54] and Zhai et al. [56], Kapoor [57] respectively), the calculated standoff distances are validated according to an "a-priori" approach. This reflects a consolidated practice in quantitative risk assessment, where risk figures are evaluated by combination of constitutive models validated a-priori. An "a-posteriori" validation process through an experimental campaign reproducing the set-up considered in the present analysis may be part of future developments to further strengthen the results.

With reference to Table 5, atmospheric vertical cylindrical storage vessels a.1–10 resulted to be inherently safe from a shooting attack with a FB2 handgun projectile as the ballistic limit velocity required is always higher than the muzzle velocity of the projectile (u_m=400 m/s). The same outcome was found considering FB4 handgun projectiles, with the only exception of vessel a.2 for which a SOD_0 of 6 m was calculated. Thus, in the case of this vessel, a successful attack can only be carried out if the shooter enters the site and reaches the interior area where the tank is located. Much higher standoff distances (order of hundreds of meters) were obtained for rifle projectiles (FB5, FB6, and FB7). Values of about 1000 metres or more were obtained for FB7 hard-core projectiles fired against small diameter tank (vessels a.1–3). Clearly, given the high values of SOD_0, the shooter may not need to enter the industrial site to carry out a successful shooting attack. However, while all the considered atmospheric storage vessels can be perforated by a FB7 projectile fired at

Table 5
Ballistic limit velocity (u_b) and maximum standoff distance (SOD_0) evaluated for the selected atmospheric storage tanks (Table 2). FB-codes defined in Table 1; IS: target is inherently safe.

ID	t_{eff} (mm)	FB2 $u_m = 400\ m/s$		FB4 $u_m = 440\ m/s$		FB5 $u_m = 950\ m/s$		FB6 $u_m = 830\ m/s$		FB7 $u_m = 820\ m/s$	
		u_b (m/s)	SOD_0 (m)	u_b (m/s)	SOD_0 (m)	u_b (m/s)	SOD_0 (m)	u_b (m/s)	SOD_0 (m)	u_b (m/s)	SOD_0 (m)
a.1	4.7	534	IS	452	IS	635	307	512	522	335	930
a.2	4.3	500	IS	423	6	594	360	479	589	318	1000
a.3	3.8	456	IS	386	IS	542	420	436	683	296	1130
a.4	4.7	534	IS	452	IS	635	307	512	522	335	930
a.5	6.9	713	IS	603	IS	847	94	683	225	421	680
a.6	8.1	804	IS	680	IS	956	IS	770	90	465	580
a.7	12.5	1113	IS	942	IS	1323	IS	1066	IS	609	320
a.8	10.1	948	IS	803	IS	1128	IS	908	IS	532	450
a.9	7.9	789	IS	667	IS	938	15	756	112	457	600
a.10	9.2	884	IS	748	IS	1052	IS	847	IS	502	510

Table 6
Ballistic limit velocity (u_b) and maximum standoff distance (SOD_0) evaluated for the selected pressurized storage tanks (Table 3). FB-codes defined in Table 1; IS: target is inherently safe.

ID	t_{eff} (mm)	FB2 $u_m = 400\ m/s$		FB4 $u_m = 440\ m/s$		FB5 $u_m = 950\ m/s$		FB6 $u_m = 830\ m/s$		FB7 $u_m = 820\ m/s$	
		u_b (m/s)	SOD_0 (m)	u_b (m/s)	SOD_0 (m)	u_b (m/s)	SOD_0 (m)	u_b (m/s)	SOD_0 (m)	u_b (m/s)	SOD_0 (m)
p.1	7.8	781	IS	661	IS	929	23	748	120	454	605
p.2	7.2	736	IS	623	IS	875	70	705	190	432	650
p.3	7.2	736	IS	623	IS	875	70	705	190	432	650
p.4	9.6	913	IS	773	IS	1086	IS	875	IS	516	485
p.5	10.3	962	IS	814	IS	1144	IS	922	IS	539	440
p.6	9.1	877	IS	742	IS	1043	IS	840	IS	499	515
p.7	12.0	1079	IS	913	IS	1283	IS	1034	IS	593	350
p.8	9.8	927	IS	785	IS	1103	IS	888	IS	522	470
p.9	8.9	863	IS	730	IS	1026	IS	826	5	492	530
p.10	9.7	920	IS	779	IS	1094	IS	881	IS	519	480
p.11	12.8	1133	IS	959	IS	1347	IS	1085	IS	618	305
p.12	14.1	1218	IS	1031	IS	1448	IS	1167	IS	657	240
p.13	12.2	1093	IS	925	IS	1299	IS	1047	IS	599	335
p.14	15.9	1333	IS	1128	IS	1585	IS	1277	IS	710	160
p.15	11.7	1059	IS	896	IS	1259	IS	1014	IS	584	360
p.16	10.7	990	IS	838	IS	1178	IS	949	IS	552	420
p.17	12.1	1086	IS	919	IS	1291	IS	1040	IS	596	340
p.18	15.0	1276	IS	1080	IS	1517	IS	1222	IS	684	200
p.19	17.9	1457	IS	1233	IS	1732	IS	1395	IS	767	75
p.20	15.2	1289	IS	1090	IS	1532	IS	1234	IS	690	190
p.21	19.9	1577	IS	1335	IS	1876	IS	1511	IS	823	IS

Table 7
Baseline standoff distances (m) proposed for generic steel atmospheric and pressurized storage tanks considering different classes of projectiles. FB-codes defined in Table 1.

SOD_0 [m]	FB2 projectiles	FB4 projectiles	FB5 projectiles	FB6 projectiles	FB7 projectiles
Atmospheric storage vessel	No perforation	6	420	685	1130
Pressurized storage vessel	No perforation	No perforation	70	190	650

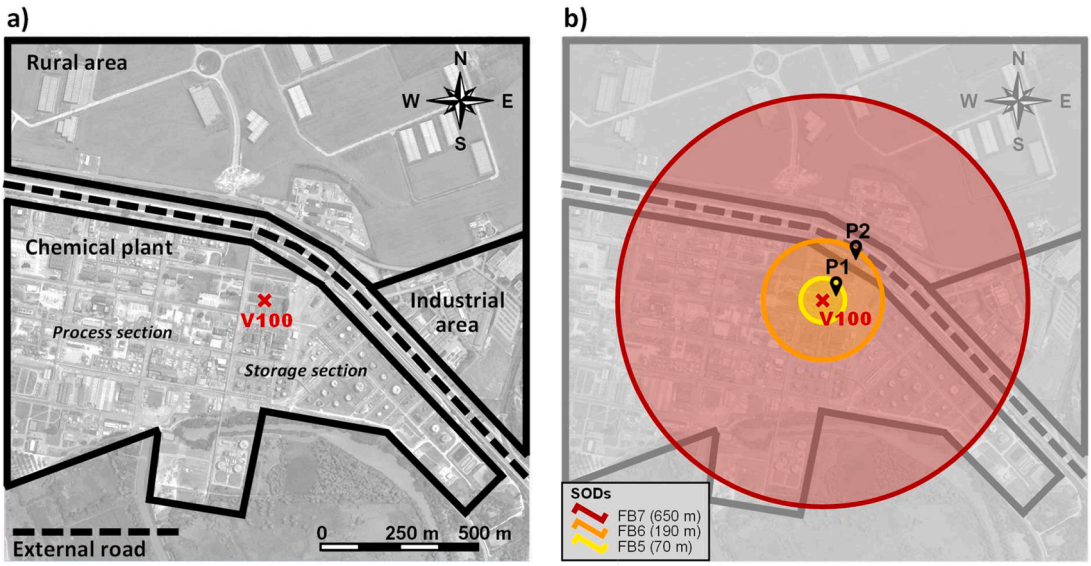

Fig. 8. a) Layout of the case study showing the position of the ammonia pressurized tank V100 considered in the analysis; b) Standoff distances corresponding to FB5, FB6, and FB7 projectiles (see Table 1) from tank V100.

distances lower than the calculated SOD_0, some of them are inherently safe from shooting attacks carried out with FB5 and FB6 projectiles (respectively a.6, a.7, a.8, a.10, and a.7, a.8, a.10).

The totality of pressurized horizontal cylindrical storage vessels considered in the present study resulted inherently safe against shooting attacks with handgun projectiles (FB2 and FB4) as reported in Table 6. Due to the greater shell thickness compared to that of atmospheric storage tanks, most of the pressurized vessels are inherently safe also from impacts with FB5 (p.4–21) and FB6 (p.4–8 and p.10–21) rifle projectiles. Vessel p.21 is inherently safe also from a shooting attack making use of a FB7 projectile.

Overall, the standoff distances obtained for the pressurized storage vessels are significantly lower than those calculated for the atmospheric storage vessels: in case of FB5 projectiles, since values of SOD_0 are in the order of tens of meters, the adversaries are required to enter the site area to carry out a successful shooting attack. On the contrary, in case of FB6 and FB7 projectiles (values of SOD_0 in the order of hundreds of meters) also attacks from outside the site may be successful.

Generic and conservative (safe-side) standoff distances are proposed for each standardized projectile considering the highest SOD_0 between those reported in Tables 5 and 6 for the analysed set of atmospheric and pressurized storage vessels. These values are reported in Table 7 and can be taken as reference standoff distances to be used by authorities and practitioners in the context of SVA/SRA to assess the vulnerability of atmospheric and pressurized storage tanks to shooting attacks. In the case of critical targets (e.g., tanks storing relevant quantities of highly hazardous materials such as liquid chlorine), the method described in Section 2 may be applied to the specific geometry, allowing for the calculation of case-specific standoff distances.

4. Application of the results to the support of SVA/SRA methodologies

A case study addressing the analysis of the storage section of a chemical plant bordering an industrial area and a rural area (see the layout in Fig 8-a) is proposed to demonstrate the use of the results to the support of SVA/SRA methodologies. In particular, the main steps of the CCPS Security Vulnerability Assessment methodology [18], which is a SVA method specific for the Chemical and Process Industry (CPI), are applied to the case study.

For the sake of conciseness, a single pressurized horizontal cylindrical tank (labelled V100 in Fig 8-a) is analysed in the case study (Critical Assets Identification – Step 2.1 of CCPS methodology).

The tank geometry and design of tank p.3 in Table 3 (P_d=1.5 MPa, V=20 m3, D=1.5 m, t=12 mm, t_d=4.8 mm, t_{eff}=7.2 mm) were considered for vessel V100. The tank was considered to store ammonia as saturated liquid at ambient temperature. Toxic dispersion is considered as the reference final scenario in case of ammonia release [13,79] (Hazards Identification – Step 2.2 of CCPS methodology).

The potential adversary considered for the facility analysed is a criminal or terrorist who shoots having V100 as a target (Adversary Identification – Step 3.1 of CCPS methodology). The characterization of the shooter (i.e., the definition of the DBT) requires the definition of the shooter capabilities, motivations, and types of firearms used (Adversary Characterization – Step 3.2 of CCPS methodology). The shooter is assumed highly capable and well-motivated. The credible set of reference firearms to be used in the DBT definition (see Section 2.2) includes all those identified in the present study: handgun firing FB2 and FB4 projectiles and/or a rifle firing FB5, FB6, and FB7 projectiles (Table 1). It is assumed that the analysis of the attractiveness of the facility (Evaluation of Target Attractiveness – Step 2.4 of CCPS methodology) yields to consider of concern the use of all the 5 projectile types identified above, both as single shot and as multiple shots (two and four projectiles fired).

A continuous release from a 11 mm hole, corresponding to the highest projectile diameter considered, was conservatively assumed in all the cases of single projectile perforation of V100. In case of multiple shots, the release rate was considered equal to the one from a single projectile hole multiplied by the number of shots.

The toxic dispersions (physical damage scenarios that follow a successful shooting attack to tank V100) were modelled using well-established literature models [33,80,81]. Atmospheric temperature of 20 °C, relative humidity of 70%, wind speed of 5 m/s at 10 m elevation, and stability Pasquill class D were assumed in the analysis of consequences. The applicable probit equation was retrieved from the "Yellow Book" of the TNO [81] and was used for the calculation of toxic effects on humans. A uniform population density was assumed equal to 40 persons/ha with 60% presence probability according to the values reported in the "Green Book" of TNO [82] for industrial areas. The expected number of fatalities was calculated using the ARIPAR methodology [83].

An "asset-based approach" (threats and hazards of the assets on site are only broadly described without exploring the specific details of all the possible attack paths) was applied as suggested by many SVA/SRA methodologies suitable for the CPI.

The main results obtained in the analysis of the case study are summarized in Table 8 and may be used to support the vulnerability and risk assessment phases in SVA/SRA (e.g., Vulnerability Analysis – Step 4 of CCPS methodology) studies.

The results in Table 8 show that, in case of a single projectile perforating tank V100, 4 fatalities are expected from the consequent ammonia toxic dispersion (three more fatalities than the maximum number that may be caused by the same projectile being directly fired on human targets). About 10 and about 19 fatalities are expected if the tank is perforated by two and four projectiles respectively (see Table 8). The high values of the expected number of fatalities are due to the extended downwind distances that can be reached by hazardous ammonia concentrations (IDLH – 300 ppm – up to 500 m downwind in case of four holes).

The last part of a SVA/SRA study (e.g., Identify Countermeasures – Step 5 of CCPS methodology) requires the analysis of the adequacy of the existing physical protection elements of the PPS (e.g., detection elements such as exterior and interior sensors, delay elements such as the fence and entry points, etc.) to manage the risk posed by the identified threats (the shooting threat in the specific case). Therefore, the recognition of the possible attack scenarios is of paramount importance in the identification of the physical protection elements in place aimed at

Table 8
Results of the consequence and vulnerability assessment steps for the identified attack scenarios.

Attack scenario	Release rate [kg/s]	Physical damage scenario	Maximum downwind distance of the plume @ 300 ppm concentration [m]	Expected number of fatalities
Single shoot	1.9	Toxic dispersion	250	4
Multiple shots (two)	3.8	Toxic dispersion	350	10
Multiple shots (four)	7.6	Toxic dispersion	500	19

detecting, deterring, and/or delaying such attacks. The baseline safe-side standoff distances provided in the present study (see Table 7) for pressurized storage vessels (such as V100) may support this phase. Actually, adversaries can succeed in perforating V100 in each of the shooting attack scenarios identified in Table 8 only in case they are able to shoot from a distance lower than the SOD_0 associated to the projectile fired. The baseline SOD_0 values applied to tank V100 for the different projectile classes are shown in Fig 8-b. Standoff distances for FB2 and FB4 projectiles are not reported as circles in the figure since, as discussed above (see Section 3.3), pressurized storage vessels are inherently safe from perforation by these two classes of projectiles. Therefore, a shooter firing with a handgun (FB2 and FB4 projectiles) is not expected to cause damage at any distance from tank V100. Thus, this case should be excluded from the list of possible attack scenarios.

Fig 8-b allows to identify two areas of intervention to improve the PPS. The first concerns a shooter that need to enter the storage section of the chemical plant in order to carry out the desired attack: this is the case of adversaries shooting FB5 rifle projectiles as they have to reach a point inside the yellow circle in Fig 8-b (e.g., point P1 in the figure) for a successful attack. These adversaries may access the site through the fence (e.g., by climbing or cutting it) or through the entrance gate of the site (e.g., by crossing with counterfeit authorization or climbing it). The perimeter fence, the credential check at the manned reception, the surveillance patrolling, and the interior video cameras are thus protection elements effective in detecting, deterring, and delaying this type of adversary.

The second area of intervention concerns shooting attacks with rifles firing FB6 or FB7 projectiles. This type of attack may be carried out even from outside the perimeter of the storage section (e.g., from point P2 in Fig 8-b), which is accessible by the external road. Based on the specific class of projectile fired, the distance of the adversary from tank V100 may include different external features (e.g., roads, buildings, fields, etc.). Exterior Video Motion Detection cameras integrated to a Closed-Circuit Television (CCTV) along the fence line are an example of an effective intrusion detection system for a shooting attack from outside the chemical plant boundaries.

The information on the credible attack scenarios and effective physical protection elements is also important in the definition of the emergency response and mitigation plans, both internal (evacuation plan) and external (population sheltering). As an example, the presence of adversaries on site may require specific checks and specific communications concerning the suitable evacuation routes.

Overall, this case study shows the criticality of the shooting threat against equipment storing hazardous materials and thus the importance of considering this threat within a SVA/SRA study. Moreover, the baseline standoff distances obtained are suitable to support the application of specific steps of SVA/SRA methodologies, as demonstrated for the CCPS methodology.

5. Conclusions

Baseline standoff distances (SOD) for shooting attacks to steel-made atmospheric and pressurized cylindrical storage vessels were calculated for a representative set of light weapon projectiles (from EN 1522 and EN 1063) using a novel approach based on validated models for projectile perforation and flight. The values obtained for the standoff distances span from less than 10 m in case of handguns, up to 685 m in case of rifles with soft-core (lead, with steel penetrator) bullets, and to 1130 m in case of rifles with hard-core (steel with full copper alloy jacket) bullets.

The effect of the initial offset angle of the shooter was studied by a Monte Carlo analysis based on credible offset angles for the considered projectile classes. The results show that appreciable variations of the standoff distance compared to the case of normal incidence of the projectile are possible only for handgun projectiles fired at targets having a small diameter (vessels with diameter of 1 m). This suggests that the adoption of probabilistic criteria for definition of SOD (e.g., based on probability of exceedance – PE – of 1%) do not significantly affect the values of the standoff distances. Thus, the use of a deterministic inherent safety approach to calculate the SOD, assuming a normal impact of the projectile on vessel wall, is advised in SVA/SRA studies.

The application of the identified reference standoff distances to a case study (storage section of a chemical plant) proved the criticality of the shooting threat against equipment storing hazardous materials as well as the potential application of the results obtained in the present analysis to support SVA/SRA methodologies and the design of the Physical Protection System (PPS) of a plant.

The approach developed, able to provide baseline standoff distances for shooting attacks, constitutes an advancement with respect to current open literature where only studies concerning the vulnerability of equipment to attacks involving explosives and arson are present. As such, it allows supporting several activities in the context of SVA/SRA, including the design of the Physical Protection System (PPS), the identification of credible scenarios, and the assessment of target vulnerability. Thus, the novel method developed, and the baseline standoff distances obtained, represent a further step towards the protection of industrial facilities from deliberate malicious attacks.

CRediT authorship contribution statement

Matteo Iaiani: Conceptualization, Formal analysis, Investigation, Methodology, Writing – original draft. **Riccardo Sorichetti:** Formal analysis, Investigation. **Alessandro Tugnoli:** Conceptualization, Methodology, Supervision, Writing – review & editing. **Valerio Cozzani:** Conceptualization, Supervision, Writing – review & editing.

Declaration of Competing Interest

The authors declare that they have no known competing financial interests or personal relationships that could have appeared to influence the work reported in this paper.

Data availability

Data will be made available on request.

Acknowledgments

This study was supported by Ministero dello Sviluppo Economico (MISE), Direzione Generale per le Infrastrutture e la Sicurezza dei Sistemi Energetici e Geominerari (DGISSEG) and by INAIL (Istituto Nazionale per l'Assicurazione contro gli Infortuni sul Lavoro).

Appendix A: Trajectory calculation by the Siacci method

The Siacci method is one of the most used approximate methods for flat-fire trajectory calculations [55]. A flat-fire trajectory is defined as a trajectory that is restricted to lie everywhere close to the x-axis (i.e., y- and z- velocity components are much smaller than the x- component). Three main assumptions are made in the Siacci method:

1. the difference in height of the lowest and highest points of the trajectory is small enough that the air density may be assumed to be constant along the trajectory;
2. the air temperature along the trajectory is constant and differs insignificantly from the standard air temperature;
3. the value of the velocity, u, is very well approximated by $u_x \sec\gamma_0$ (called "pseudo-velocity") along the entire trajectory, where u_x is the horizontal component of the velocity and $\sec\gamma_0$ is the secant of the angle of departure in the vertical plane.

Starting from Newton's second law of motion for a planar trajectory acted on by the forces of aerodynamic drag and gravity, and considering the formulation above of the pseudo-velocity, it is possible to derive the Siacci differential equation of the time-of-flight function, of the space function, of the inclination function, and of the altitude function. The details on the derivation of each Siacci differential equation can be found in [55].

Given the aim of the present study to provide standoff distances for atmospheric and pressurized storage vessels with reference to a representative set of light weapon projectiles, the Siacci space differential equation was used in the calculations. The equation is the following:

$$\frac{d(d_r)}{du} = \frac{-C\cos(\gamma_0)}{G(u)} \tag{A.1}$$

where d_r is the downrange distance, C is the ballistic coefficient, and $G(u)$ is the drag function.

The utility of the Siacci method is based on the use of numerical quadrature to tabulate four primary functions, which are the solutions of the Siacci differential equations. In particular, the Siacci primary function of interest is the downrange distance travelled or space function $S(u)$, defined as:

$$S(u) = \int_{u}^{u_{max}} \frac{du}{G(u)} \tag{A.2}$$

where u_{max} is the maximum velocity, taken equal to the muzzle velocity (u_m).

$S(u)$ is numerically tabulated for the most common drag functions (named G_1, G_2, G_5, G_6, G_7, and G_8) and for a wide set of velocities (from 4500 ft/s down to 100 ft/s, in 10 ft/s intervals): the reader is referred to [55] where the tables are reported.

Integrating equation (A.1) and substituting equation (A.2) yields:

$$d_r(u) = C\cos(\gamma_0)[S(u) - S(u_m)] \tag{A.3}$$

For short ranges and very flat-fire trajectories, $\cos(\gamma_0) \approx 1$, and equation (A.3) becomes:

$$d_r(u) \cong C[S(u) - S(u_m)] \tag{A.4}$$

Clearly enough, the standoff distance (SOD) is equal to the downrange distance calculated at the ballistic limit velocity (u_b):

$$SOD = C[S(u_b) - S(u_m)] \tag{A.5}$$

Ballistic coefficients and respective drag functions used for the set of projectiles considered in this study are reported in Table A.1.

Table A.1
Ballistic coefficients and respective drag functions for the selected projectiles.

Protection Class	Type of weapon	Reference projectile	Projectile type	u_m (m/s)	Ballistic Coefficient C (lb/in^2)	Drag Function
FB2	Handgun	9 mm Luger	RN/SC	400	0.135	G_1
FB4	Handgun	44 Rem. Mag.	FN/SC	440	0.185	G_1
FB5	Rifle	5.56×45	PB/SC	950	0.151	G_7
FB6	Rifle	7.62×51	P/SC	830	0.200	G_7
FB7	Rifle	7.62×51	FP/HC	820	0.200	G_7

Appendix B: Monte Carlo simulations

The Monte Carlo method (see the typical steps in Fig B.1-a) was applied in order to investigate the effect of the initial offset angle of the shooter on the standoff distance. The simulations were carried out for each projectile class considered in the present study, i.e., FB2, FB4, FB5, FB6, and FB7 projectiles (see Table 1 in Section 2.2) and were all referred to the case of target diameter (D) equal to 1 m (worst-case diameter scenario for storage vessels). In fact, the effect of the offset angle on SOD increases as the target diameter decreases, and 1 m is the minimum amongst the diameters of the atmospheric and pressurized storage vessels considered as target elements in the current analysis (see Section 2.2).

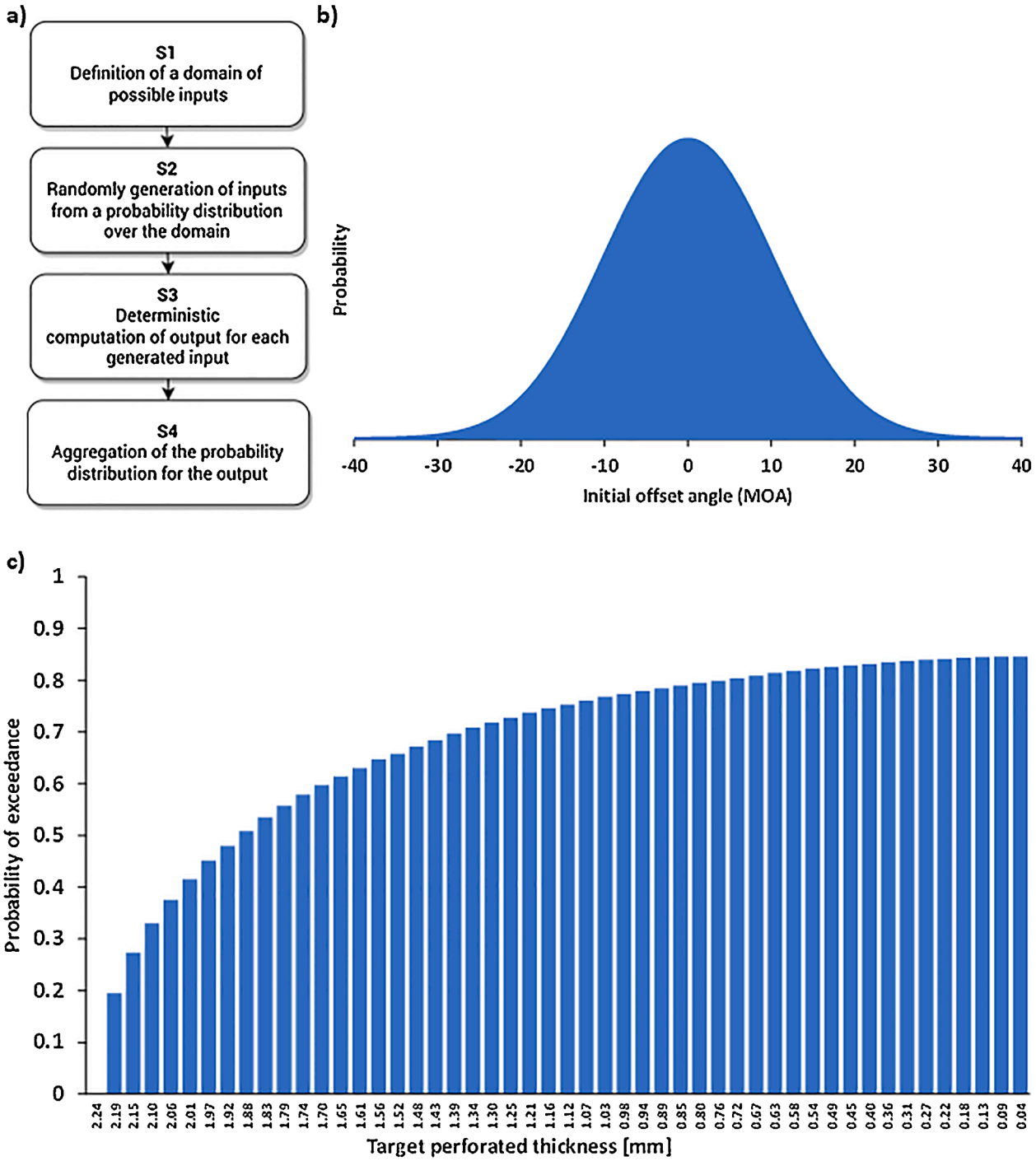

Fig. B.1. a) Steps of a Monte Carlo method; b) Example of normal distribution for offset angle used as input in Monte Carlo simulation (mean: 0 MOA; standard deviation: 10 MOA); c) Example of results obtained for probability of exceedance of vessel perforation for different classes of target perforated thickness (horizontal axis reports the mm value of the upper bound of the class) for a given projectile type, target diameter, and downrange distance.

The initial offset angles (ϕ) measured in MOA (Minute of Angle) were chosen as the input parameters in the Monte Carlo simulations (see S1 in Fig B.1-a). In order to randomly generate ϕ values (see S2 in Fig B.1-a), a normal distribution of central value 0 and standard deviation of ϕ_r /2 was assumed as the probability density function for the initial offset angle. ϕ_r was taken equal to 20 MOA for handgun projectiles and 1 MOA for rifle projectiles (see Section 2.2). Use of $\phi_r/2$ as standard deviation in a normal distribution guarantees that 95% of initial offset angles are within ϕ_r. An example of normal probability density function with central value 0 and standard deviation of 10 MOA (i.e., the case of FB2 and FB4 projectiles) is shown in Fig B.1-b.

Once the probability distribution was set up, 10,000 offset angles were randomly generated, and the corresponding target perforated thickness was calculated for discrete values of the distance from the target (see S3 in Fig B.1-a). The deterministic computation was based on the solution of the system of Eqs. (1), (2), (9), (10), and (11) reported in the main text.

This way, at a given distance from the target, for each generated offset angle, the corresponding target perforated thickness was calculated, allowing to obtain the probability of exceedance (PE) of vessel perforation (Fig B.1-c shows the one obtained for FB2 projectiles at a distance from the

target equal to 120 m). PE of 1%, 5%, 10%, 30%, and 50% was considered. For example, with reference to Fig B.1-c, the target perforated thickness corresponding to PE of 30% is 2.12 mm: this means that, firing with a FB2 projectile at 120 m from the target, a thickness of 2.12 mm or higher is perforated in 30% of cases. Thus, 120 m is the standoff distance with a probability of exceedance of 30%, indicated as SOD_{30}, for FB2 projectiles.

Finally, the graphs shown in Fig B.2 were obtained by plotting the target penetrated thickness for the probability of exceedance of interest vs. the considered discrete value of the downrange distance of the target. Each graph reports 6 curves: one refers to the case of normal incidence (black line), while the other five curves refer to the probability of exceedance of 1% (orange line), 5% (grey line), 10% (red line), 30% (blue line), and 50% (green line), named PE1, PE5, PE10, PE30, PE50 respectively.

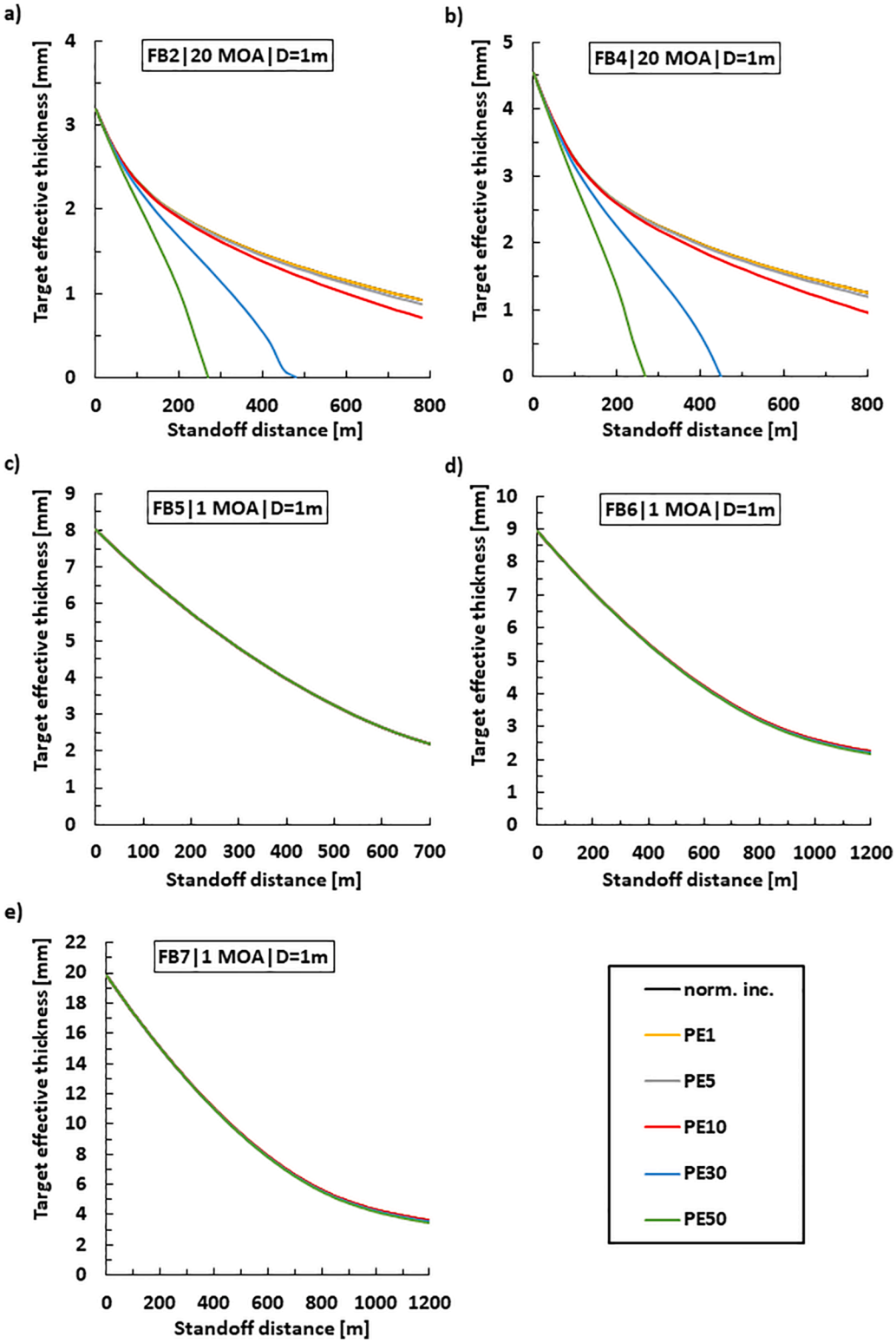

Fig. B.2. Results of Monte Carlo simulations considering target diameter (***D***) of 1 m for: a) FB2 projectiles; b) FB4 projectiles; c) FB5 projectiles; d) FB6 projectiles; e) FB7 projectiles.

References

[1] Landucci G, Reniers G. Preface to special issue on quantitative security analysis of industrial facilities. Reliab Eng Syst Saf 2019;191:106611. https://doi.org/10.1016/j.ress.2019.106611.

[2] Baybutt P. 3. Security vulnerability analysis: protecting process plants from physical and cyber threats. Security Risk Assessment in The Chemical and Process Industry, de Gruyter 2017:31–74. https://doi.org/10.1515/9783110499087-003.

[3] Reniers G. Terrorism security in the chemical industry: Results of a qualitative investigation. Secur J 2011;24:69–84. https://doi.org/10.1057/sj.2009.10.

[4] van Staalduinen MA, Khan F, Gadag V, Reniers G. Functional quantitative security risk analysis (QSRA) to assist in protecting critical process infrastructure. Reliab Eng Syst Saf 2017;157:23–34. https://doi.org/10.1016/j.ress.2016.08.014.

[5] Song G, Khan F, Yang M. Probabilistic assessment of integrated safety and security related abnormal events: a case of chemical plants. Saf Sci 2019;113:115–25. https://doi.org/10.1016/j.ssci.2018.11.004.

[6] Bajpai S, Gupta JP. Terror-proofing chemical process industries. Process Saf Environ Prot 2007;85:559–65. https://doi.org/10.1205/psep06046.

[7] Casson Moreno V, Reniers G, Salzano E, Cozzani V. Analysis of physical and cyber security-related events in the chemical and process industry. Process Saf Environ Prot 2018;116:621–31. https://doi.org/10.1016/j.psep.2018.03.026.

[8] Iaiani M, Casson Moreno V, Reniers G, Tugnoli A, Cozzani V. Analysis of events involving the intentional release of hazardous substances from industrial facilities. Reliab Eng Syst Saf 2021;212:107593. https://doi.org/10.1016/J.RESS.2021.107593.

[9] Iaiani M, Tugnoli A, Bonvicini S, Cozzani V. Analysis of Cybersecurity-related Incidents in the Process Industry. Reliab Eng Syst Saf 2021;209:107485. https://doi.org/10.1016/j.ress.2021.107485.

[10] Chen C, Reniers G, Khakzad N. Integrating safety and security resources to protect chemical industrial parks from man-made domino effects: A dynamic graph approach. Reliab Eng Syst Saf 2019;191:106470. https://doi.org/10.1016/j.ress.2019.04.023.

[11] Zhu R, Hu X, Bai Y, Li X. Risk analysis of terrorist attacks on LNG storage tanks at ports. Saf Sci 2021;137:105192. https://doi.org/10.1016/j.ssci.2021.105192.

[12] Cozzani V, Gubinelli G, Antonioni G, Spadoni G, Zanelli S. The assessment of risk caused by domino effect in quantitative area risk analysis. J Hazard Mater 2005;127:14–30. https://doi.org/10.1016/j.jhazmat.2005.07.003.

[13] Iaiani M, Tugnoli A, Cozzani V. Identification of reference scenarios for security attacks to the process industry. Process Saf Environ Prot 2022;161:334–56. https://doi.org/10.1016/j.psep.2022.03.034.

[14] Störfall-Kommission (SFK). SFK–GS–38 - Combating Interference by Unauthorised Persons 2002.

[15] Pasman H. 2. American legislation and regulatory measures: a lesson for Europe? Security Risk Assessment in The Chemical and Process Industry, de Gruyter; 2017, p. 6–30. https://doi.org/10.1515/9783110499087-002.

[16] Guikema SD, Aven T. Assessing risk from intelligent attacks: A perspective on approaches. Reliab Eng Syst Saf 2010;95:478–83. https://doi.org/10.1016/J.RESS.2009.12.001.

[17] Matteini A, Argenti F, Salzano E, Cozzani V. A comparative analysis of security risk assessment methodologies for the chemical industry. Reliab Eng Syst Saf 2019;191:106083. https://doi.org/10.1016/j.ress.2018.03.001.

[18] Center for Chemical Process Safety (CCPS). Guidelines for Analyzing and Managing the Security Vulnerabilities of Fixed Chemical Sites 2003.

[19] Jaeger CD. Vulnerability assessment methodology for chemical facilities (VAM-CF). Chem Health Saf 2002;9:15–9. https://doi.org/10.1016/S1074-9098(02)00389-1.

[20] American Petroleum Institute (API). API RP 780: Security Risk Assessment Methodology for the Petroleum and Petrochemical Industries 2013.

[21] Moore DA, Fuller B, Hazzan M, Jones JW. Development of a security vulnerability assessment process for the RAMCAP chemical sector. J Hazard Mater 2007;142:689–94.

[22] Landucci G, Argenti F, Cozzani V, Reniers G. Assessment of attack likelihood to support security risk assessment studies for chemical facilities. Process Saf Environ Prot 2017;110:102–14. https://doi.org/10.1016/j.psep.2017.06.019.

[23] Argenti F, Landucci G, Reniers G, Cozzani V. Vulnerability assessment of chemical facilities to intentional attacks based on Bayesian Network. Reliab Eng Syst Saf 2018;169:515–30. https://doi.org/10.1016/j.ress.2017.09.023.

[24] Feng Q, Cai H, Chen Z. Using game theory to optimize the allocation of defensive resources on a city scale to protect chemical facilities against multiple types of attackers. Reliab Eng Syst Saf 2019;191:105900. https://doi.org/10.1016/J.RESS.2017.07.003.

[25] Rezazadeh A, Talarico L, Reniers G, Cozzani V, Zhang L. Applying game theory for securing oil and gas pipelines against terrorism. Reliab Eng Syst Saf 2019;191:106140. https://doi.org/10.1016/J.RESS.2018.04.021.

[26] Hausken K. Security Investment, Hacking, and Information Sharing between Firms and between Hackers. Games (Basel) 2017;8:23. https://doi.org/10.3390/g8020023.

[27] Khakzad N, Reniers G. Low-capacity utilization of process plants: A cost-robust approach to tackle man-made domino effects. Reliab Eng Syst Saf 2019;191:106114. https://doi.org/10.1016/J.RESS.2018.03.030.

[28] Abdo H, Flaus JM, Masse F, Abdo H, Flaus JM, Masse F. Fuzzy semi-quantitative approach for probability evaluation using Bow-Tie analysis. HAL Archives-Ouvertes 2017:2597–605.

[29] Casson Moreno V, Marroni G, Landucci G. Probabilistic assessment aimed at the evaluation of escalating scenarios in process facilities combining safety and security barriers. Reliab Eng Syst Saf 2022;228. https://doi.org/10.1016/j.ress.2022.108762.

[30] IAEA- International Atomic Energy. Defence in depth in nuclear safety. Vienna: 1996.

[31] Landucci G, Reniers G, Cozzani V, Salzano E. Vulnerability of industrial facilities to attacks with improvised explosive devices aimed at triggering domino scenarios. Reliab Eng Syst Saf 2015;143:53–62. https://doi.org/10.1016/j.ress.2015.03.004.

[32] Garcia M.L. The design and evolution of physical protection systems. 2nd ed. Butterworth-Heinemann; 2007.

[33] Mannan S. Lees' Loss Prevention in the Process Industries: Hazard Identification. Assessment and control. 4th ed. UK: Butterworth-Heinemann: Elsevier; 2012.

[34] Gouller. Safety distances, zones of protection and receiving basins for the storage of liquefied gases. Prevention of Occupational Risks 1970;1.

[35] Laska. Safety distances in great storage zones of dangerous gases. Prevention of Occupational Risks 1970;1.

[36] Healy F. Notes on the Basis of Outside Safety Distances for Explosives Involving the Risk of Mass Explosion. Rep. 3/7/EXPLOS/43. 1959.

[37] Jarrett DE. Derivation of the British explosives safety distances. Ann N Y Acad Sci 1968;152:18–35. https://doi.org/10.1111/J.1749-6632.1968.TB11963.X.

[38] Mercx WPM, Weerheijm J, Verhagen TLA. Some considerations on the damage criteria and safety distances for industrial explosions. Hazards XI 1991;255.

[39] Schonbucher A, Gock D, Fiala R. Prediction of the heat radiation and safety distances for large fires with the model OSRAMO. Loss Prevention and Safety Promotion 1992;7.

[40] Dusso A, Grimaz S, Salzano E. Quick assessment of fire hazard in chemical and pharmaceutical warehouses. Chem Eng Trans 2016;48:325–30. https://doi.org/10.3303/CET1648055.

[41] Qin H, Stewart MG. Casualty Risks Induced by Primary Fragmentation Hazards from High-explosive munitions. Reliab Eng Syst Saf 2021;215. https://doi.org/10.1016/j.ress.2021.107874.

[42] Dong M, Zhang Z, Liu Y, Zhao DF, Meng Y, Shi J. Playing Bayesian Stackelberg game model for optimizing the vulnerability level of security incident system in petrochemical plants. Reliab Eng Syst Saf 2023;235. https://doi.org/10.1016/j.ress.2023.109237.

[43] Kumar S, Saxena S, Sharma H, Gangolu J, Prabhu TA. Development of design guidelines using probabilistic framework for the development of smart thickening fluid based ultra resistant adaptive kinematic soft human armor (SURAKSHA). Reliab Eng Syst Saf 2023;236. https://doi.org/10.1016/j.ress.2023.109277.

[44] Anderson CE. Analytical models for penetration mechanics: A Review. Int J Impact Eng 2017;108:3–26. https://doi.org/10.1016/j.ijimpeng.2017.03.018.

[45] Stewart MG, Netherton MD. Statistical variability and fragility assessment of ballistic perforation of steel plates for 7.62 mm AP ammunition. Defence Technology 2020;16:503–13. https://doi.org/10.1016/j.dt.2019.10.013.

[46] Schonberg W, Ryan S. Predicting metallic armour performance when impacted by fragment-simulating projectiles – model review and assessment. Int J Impact Eng 2021;158:104025. https://doi.org/10.1016/j.ijimpeng.2021.104025.

[47] Schonberg W, Ryan S. Predicting metallic armour performance when impacted by fragment-simulating projectiles – Model adjustments and improvements. Int J Impact Eng 2022;161:104090. https://doi.org/10.1016/j.ijimpeng.2021.104090.

[48] Li Y, Jiang J, Yu Y, Wang Z, Xing Z, Zhang Q. Fire resistance of a vertical oil tank exposed to pool-fire heat radiation after high-velocity projectile impact. Process Saf Environ Prot 2021;156:231–43. https://doi.org/10.1016/j.psep.2021.10.013.

[49] Li X, Liao K, He G, Zhao J. Influence of blunt-nose and conical fragment on domino accident probability in spherical-tank area. Process Saf Environ Prot 2021;146:800–10. https://doi.org/10.1016/j.psep.2020.12.014.

[50] Scarponi GE, Tugnoli A, Cozzani V. 5. Projectile (missile) driven domino effect. editor. In: Khan F, editor. Domino effect : its prediction and prevention. 1st ed. Academic Press; 2021.

[51] Chen XW, Li QM. Deep penetration of a non-deformable projectile with different geometrical characteristics. Int J Impact Eng 2002;27:619–37. https://doi.org/10.1016/S0734-743X(02)00005-2.

[52] Lecysyn N, Bony-Dandrieux A, Aprin L, Heymes F, Slangen P, Dusserre G, et al. Experimental study of hydraulic ram effects on a liquid storage tank: Analysis of overpressure and cavitation induced by a high-speed projectile. J Hazard Mater 2010;178:635–43. https://doi.org/10.1016/j.jhazmat.2010.01.132.

[53] Lecysyn N, Dandrieux A, Heymes F, Aprin L, Slangen P, Munier L, et al. Ballistic impact on an industrial tank: Study and modeling of consequences. J Hazard Mater 2009;172:587–94. https://doi.org/10.1016/j.jhazmat.2009.07.086.

[54] Iaiani M, Sorichetti R, Tugnoli A, Cozzani V. Projectile perforation models for the vulnerability assessment of atmospheric storage tanks. Process Saf Environ Prot 2022;161:231–46. https://doi.org/10.1016/j.psep.2022.03.025.

[55] McCoy RL. Modern exterior ballistics. the launch and flight dynamics of symmetric projectiles. Schiffer Publishing Ltd.; 2012.

[56] Zhai XJ, Dong XD, Luo W. Exterior trajectory computation and modeling of kinetic energy ammunition based on constant terminal effect. Procedia Eng 2012;31:922–7. https://doi.org/10.1016/j.proeng.2012.01.1122.

[57] Kapoor A. Extension of Resistance Law by Approximated Function for Trajectory. Def Sci J 1980;30:113–20. https://doi.org/10.14429/dsj.30.6437.

[58] Crouch IG. Woodhead publishing in materials the science of armour materials edited by. Elsevier; 2017.

[59] Hazell PJ. Armour: materials, theory, and design. CRC Press; 2015.

[60] Børvik T, Dey S, Clausen AH. Perforation resistance of five different high-strength steel plates subjected to small-arms projectiles. Int J Impact Eng 2009;36:948–64. https://doi.org/10.1016/j.ijimpeng.2008.12.003.

[61] European Committee for Standardization (CEN). EN 1063: Glass in building - Security glazing - Testing and classification od resistance against bullet attack 2019.
[62] European Committee for Standardization (CEN). BS EN 1522: Windows, doors, shutters and blinds - Bullet resistance - Requirements and classification 1999.
[63] Chen X, Gao Y, He L. Analysis on the perforation of ductile metallic plates by APM2 bullets. Int J Prot Struct 2013;4:65–78. https://doi.org/10.1260/2041-4196.4.1.65.
[64] Stephens M, Thibault KL. Effects of bullet caliber and impact velocity on temporary cavity formation and bullet fragmentation: An experimental study. Forensic Sci Int 2016;264:121–8.
[65] Acceptable Accuracy From Different Shooting Positions | The Hunting Gear Guy n. d. https://www.huntinggearguy.com/competition/acceptable-accuracy-from-different-shooting-positions/(accessed December 19, 2022).
[66] Dan J. Precision Pair. Guns & Ammo 2005.
[67] Byrd RA. Precession Sniper Rifle - Solicitation Number 2008. H92222-09-PSR.
[68] Minute of Angle (MOA) NSSF. NssfOrg n.d. https://www.nssf.org/shooting/minute-angle-moa/ (accessed November 7, 2022).
[69] Ullmann's Encyclopedia. Ullmann's encyclopedia of industrial chemistry. 7th ed. Wiley-VCH; 2011.
[70] Cozzani V, Gubinelli G, Salzano E. Escalation thresholds in the assessment of domino accidental events. J Hazard Mater 2006;129:1–21. https://doi.org/10.1016/j.jhazmat.2005.08.012.
[71] American Petroleum Institute (API). API RP 650: Welded Tanks for Oil Storage. 13th ed. 2021.
[72] ASME ASME Boiler and Pressure Vessel Code, Section VIII, Part C. 2013.
[73] Callister W.D., Rethwisch D.G. Materials science and engineering. An indroduction. vol. 10th Editi. 2018. https://doi.org/10.1016/0025-5416(74)90116-5.
[74] Zukas JA. High velocity impact dynamics. Wiley-Interscience; 1990.
[75] Carlucci DE, Jacobson SS. Ballistics: theory and design of guns and ammunition. CRC Press/Taylor & Francis Group; 2008.
[76] Brown SJ. Energy release protection for pressurized systems. Part II. Rewiew of studies into impact/terminal ballistics. Appl Mech Rev 1986;39:177–201. https://doi.org/10.1115/1.3143704.
[77] Harvey J.F. Pressure Vessel Design: Nuclear and Chemical Applications. Van Nostrand Company; 1963.
[78] Cozzani V, Tugnoli A, Salzano E. Prevention of domino effect: From active and passive strategies to inherently safer design. J Hazard Mater 2007;139:209–19. https://doi.org/10.1016/J.JHAZMAT.2006.06.041.
[79] Uijt de Haag P.A.M., Ale B.J.M. Guidelines for quantitative risk assessment (TNO Purple Book). The Hague (NL): Committee for the Prevention of Disasters; 2005.
[80] Center of Chemical Process Safety (CCPS). Guidelines for chemical process quantitative risk analysis. New York: American Institute of Chemical Engineers - Center of Chemical Process Safety; 2000.
[81] Van Den Bosh CJH. Weterings RAPM. Methods for the calculation of physical effects (TNO Yellow Book). The hague (NL): committee for the prevention of disasters. 3rd ed. 2005.
[82] TNO - The Netherlands Organisation of Applied Scientific Research. Methods for the determination of possible damage to people and objects resulting from releases of hazardous materials (TNO green book). 1st ed. Committee for the Prevention of Disasters; 1992.
[83] Egidi D, Foraboschi FP, Spadoni G, Amendola A. The ARIPAR project: analysis of the major accident risks connected with industrial and transportation activities in the Ravenna area. Reliab Eng Syst Saf 1995;49:75–89. https://doi.org/10.1016/0951-8320(95)00026-X.